Ritsumeikan Asia Pacific University
Graduate School of Asia Pacific Studies
International Cooperation Policy
Laboratory of Environmental Geoscience
Master Thesis

Estimating CO_2 Sequestration by Forests in Oita Prefecture, Japan, Combining LANDSAT ETM+ and ALOS Satellite Remote Sensing Data

Kotaro Iizuka
(Student Number 51210012)
January 2012

Supervisor: Professor Dr. SANGA-NGOIE Kazadi

Table of Contents

List of Figures

List of Tables

Abstract

Estimation of CO_2 sequestration by the forests of Oita Prefecture, Japan, was implemented. LANDSAT ETM+ (May 25, 2002 and Dec 30, 2006) and ALOS PALSAR (Sep 15, 2009 and Oct 14, 2009) satellite remote sensing data of the study area were acquired and were analyzed with IDRISI Andes/Taiga GIS software platform. Hybrid classification was performed with a maximum likelihood method for producing a detailed land cover map and calculating the total area of the forests (coniferous, deciduous broadleaf and evergreen broadleaf forests). First, CO_2 sequestration for each forest types was calculated using the sequestration value per unit area then multiplying with the total forests area, resulting in 6.6 $MtCO_2$/yr in total. Second, for a deeper analysis, the stem volume of the forested area was estimated by using the PALSAR image to find out the tree age for each forest types in order to estimate accurate sequestration. Coniferous and deciduous broadleaf forests were classified into categories per ages and the estimation was made resulting in 2.9 $MtCO_2$/yr and 0.3 $MtCO_2$/yr for coniferous and deciduous broadleaf forests, respectively. The results have shown the importance of considering not only the forest type, but the tree age for estimating more precise CO_2 sequestration to prevent overestimation of the forests capacity.

要約

本研究は、大分県の森林が持つ二酸化炭素固定量の算定を目的にしている。LANDSAT ETM+ (2002 年 5 月 25 日と 2006 年 12 月 30 日) と ALOS PALSAR (2009 年 9 月 15 日と 2009 年 10 月 14 日) 衛星リモートセンシングデータを取得し、GIS ソフトウェア IDRISI Andes/Taiga を用いてすべての分析を行った。ハイブリッドクラシフィケーションに最尤法を用いることで、詳細な土地被覆図の作成を行い、林種別（針葉樹林、落葉広葉樹林、常緑広葉樹林）の総面積を計算した。二酸化炭素固定量の算定は、単位面積当たりの固定量を森林域の面積とで乗じることにより算出した。結果、大分県は全体で 6.6 $MtCO_2$/yr 固定することが分かった。さらに深い分析のために、PALSAR を用いた材積の推定を実施した。この材積を用いて林種別の森林域を、それぞれの林齢毎の範囲に再分類した。再分類した後、林齢毎の固定量を利用し二酸化炭素固定量を再計算した。結果、針葉樹林は 2.9 $MtCO_2$/yr、落葉広葉樹林は 0.3 $MtCO_2$/yr を固定することが分かった。これより分かったことは、詳細な土地被覆図の作成による樹種の判別と、樹種毎の林齢を考慮することで過大評価することを避け、より精確な二酸化炭素固定量を算定できるということである。

1. Introduction

1.1. Research Background

Global Warming is considered as one of the most crucial environmental issues in the 21st century. Many research and conferences have been held to emphasize the importance of this issue and associated problems, and many nations are working together on policies if not for preventing the problem, but at least for mitigating its impacts (Hewitt & Jackson, 2003; Chiras, 2006). Japan, is one of the top nations which is involving in many activities related to this issue, and the Kyoto Protocol (adopted at the Kyoto Conference in 1997) has provided a new approach to finding solutions (UNFCC, 1998). Clean Development Mechanism (CDM), Emission Trading, Joint Implementation (JI) and Carbon Sink are the main Kyoto Mechanisms, and among them carbon sink is very important in the current research context, as 68.9% of lands in Japan is covered by forests (OECD, 2004). Japan is considering the forests to be the top candidate for its CO_2 reduction process (Ministry of Economy, Trade and Industry (METI), 2005). Many prefectures in Japan have done research about the forests carbon sequestration and have come up with policies for the implementation of reducing CO_2. However, some prefectures have not yet been involved in such processes that focus on CO_2 reduction through carbon sink although they have a great amount of forest cover. Oita Prefecture is one of them.

Oita Prefectural Government has so far focused on energy conservation as the main mechanism for effectively reducing CO_2 (Oita Prefecture Global Warming Measure, 2006). The Oita Prefecture's global warming measure implementation has started in 2005, aiming at reducing energy consumption and wastes, and introducing more energy-efficient systems (co-generation system). The results of this approach (Figure.1) do not look so effective at all.

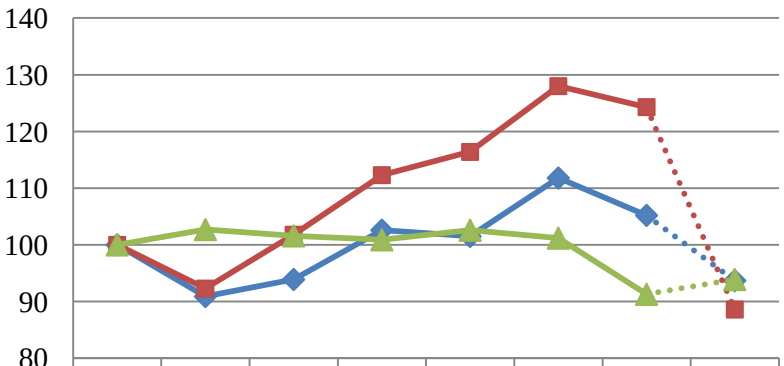

	2002 Base	2003	2004	2005	2006	2007	2008	2010 Target
Household	100	90.9	93.9	102.6	101.5	111.8	105.2	93.7
Service	100	92.3	101.8	112.3	116.4	128	124.3	88.6
Transport	100	102.7	101.6	100.9	102.6	101.2	91.3	93.9

Figure 1. Changes in CO_2 emissions from 3 targeted sectors in Oita Prefecture, with 2002 as the reference year (100%) (Oita Prefecture Global Warming Measure, 2010).

It is thus time to reconsider the measure and the tools used by the Prefectural Government for the implementation of this regulation to actually make a step forward to achieve the goals. We have to note that Oita Prefecture has not focused on reducing CO_2 through the concept of carbon sink and depending strongly on the energy efficiency which was mentioned above, showing that it is not making much progress towards the goal. The reason for this is more likely because of the lack of sound scientific data needed for objective decision making about which process to use for effectively implementing the policy in the long term.

1.2. Review of Previous Works

Traditional methods of estimating carbon/CO_2 through a site-based method (Tadaki & Hachiya, 1968; Bird, 2010) or using eddy covariance flux tower are sometimes expensive, time consuming and limits the coverage of the area. Even to expand the area or implementing continuous monitoring will be more costly and time consuming. Remotely sensed satellite observations have provided the scientists with an alternative method of the way to study the Earth's nature (atmosphere, vegetation, etc.). On the study of vegetation it has been demonstrated that the reflectance of the wavelength (red, green, infrared) radiation contains considerable information about plant biomass (Tucker, 1979), leading to the extraction of vegetation information and giving us the possibility of monitoring at lower costs and less time. Today, with further advancement of research, it is a common application not only even to produce maps to categorize the land cover type of the surface for allocating and managing the Earth's resources (Lo & Choi, 2004) but to analyze the changes and its impacts for future developments (Xiuwan, 2002). The remotely sensed method for evaluating the carbon/CO_2 sequestration have been implemented in various ways, and one is to use the land cover information to combine with the averaged carbon sequestration value of different land cover types to estimate regional sequestrations (Janssens et.al, 2003). The strength of using land cover information based on remotely sensed images is to cover regional or even global scales of the area and also it can observe sites that are difficult to access when on the ground. Moreover it allows implementation of continuous monitoring of the area for analyzing the changes of the land cover. However, it is important to determine not only the types of land cover but also the differences of the tree age can result in a big difference in the estimation (Turner et.al, 2004). The estimation implemented in Japan is more concerned at the continental scale (whole Japan) which focuses mostly at identifying the forests to the natural and the planted forests. Hiroshima & Nakajima (2006) has focused on the potential carbon sinks in Japanese plantation forests during the first commitment period of the Kyoto Protocol. They have estimated that the private planted forests were expected to sequester 8.16-8.87 MtC/yr, depending on the different scenarios of the forest management based on silvicultural practices, employing subsidies and forest workers' wages as predictor variables. Sasaki & Kim (2009) has estimated potential sequestration of the forests in Japan and the eligible sequestration under the condition of the Marrakesh Accords. Using the land use model and carbon stock growth model, it has been estimated that the forests in Japan is likely to sequester 20.1 MtC/yr (planted forests: 15.3 MtC/yr, natural: 4.8 MtC/yr), and in the conditions under the Marrakesh Accords,

it is estimated at 10.2 MtC/yr (planted forests: 7.3 MtC/yr, natural: 2.9 MtC/yr). Few studies estimates the potential of the sequestration by the forests in Japan and not many considers to perform an analysis to look through in a local or regional scale focusing more on detailed forest types, which can be understood because the Kyoto Protocol consists at the national level so many studies estimates at that scale. However, in the case of estimations performed by those authors mentioned above are based on a modeling while the information of where and how much those resources exist is not considered, which is not good because it won't give a further information of then how to make decision for treating those resources. It must also take in consider that the forests are more diverse than just a natural or planted forests. Thus it must be analyzed more on a local or regional scale locating precise and detailed classes of the forests types or the tree types for a realistic estimation of the sequestration, because tree types and even tree ages makes differences in sequestration (Tadaki & Hachiya, 1968; MAFF, 2010). After locating the precise information of the forests, we will be able to estimate the true value of the forests capacity. Once this information is obtained, it will become strong information which can be provided for important decision making on forest management and so on. To plan for future developments and taking decision for actions, the status and location of resource is a critical issue to effectively manage those resources over time.

1.3. Research Objective

The objective of this research is to re-assess the estimation of CO_2 sequestration by forests covers in Oita Prefecture based on precise evaluation of forests extents in Oita. This will make it possible to quantitatively estimate their potential storage capacity, and therefore, maximize the usage of this environmental resource as a CO_2 sink. These findings will help Oita Prefecture devise better scenarios for mitigating the global warming issue. Local and regional scale analysis of the land cover and estimation of CO_2 sequestration will eventually contribute to the updated information of Japan's CO_2 reduction target achievement.

2. Study Area and Data Sets

2.1. Oita Prefecture

The research area, Oita Prefecture, is located on the Kyushu Island at the southwestern part of Japan (Figure.2), between 130.50° E and 132.11° E, 32.43° N and 33.44° N, with a total land area of 6,339 km^2. Official figures show that 4540 km^2, which make 72 % of lands, are covered by forests (Oita Prefecture Forestry Figures, 2003).

Oita Prefecture is surrounded by several mountains ranges, up to 1758 m in altitude. Climatic conditions divide the prefecture in two main areas: (1) the area effected by the monsoon winds coming from the coast of the Japan Sea, and bringing in large amounts of rainfall and large number of rainy days in winter, and (2) the area characterized by large amounts of rains in summer resulting from the moisture flowing in from the Pacific Ocean, and by dry and fine weathers in winter. The dynamic meteorological factor of these very wet climate conditions

results annual rainfall in Oita Prefecture ranging from 1500~1600 mm over coastal areas, to 2500~3000 mm in the mountainous areas.

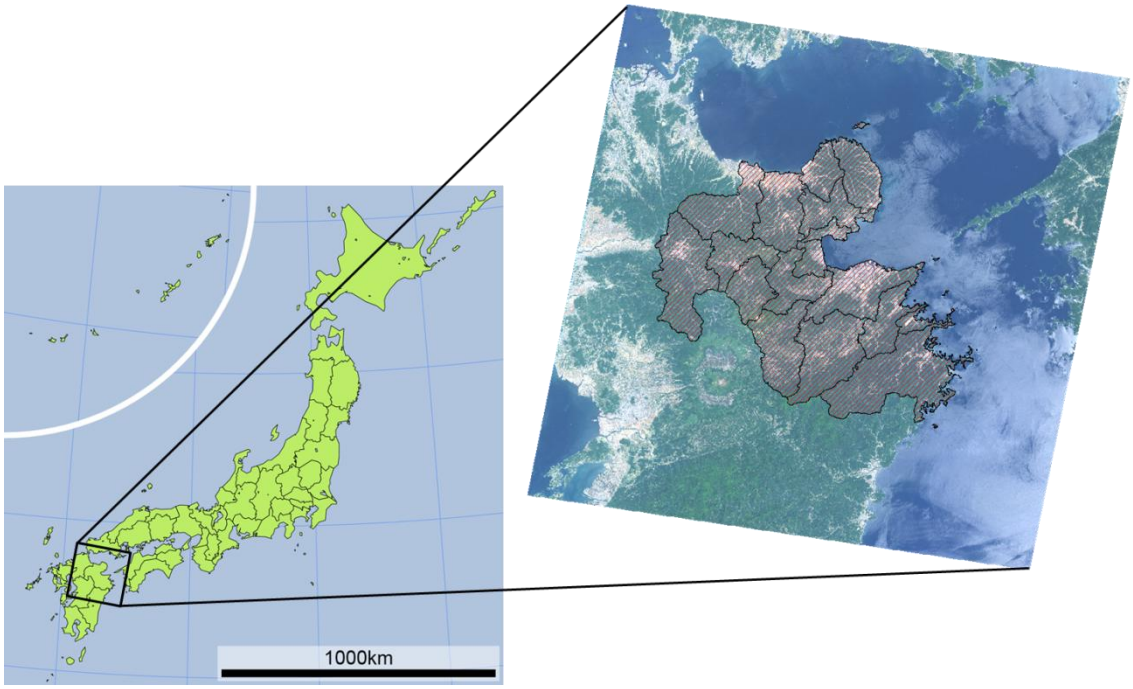

Figure 2. Location of the study area (Oita Prefecture, Japan). The enlarged image of Oita Prefecture with its administrative units (cities, towns and villages) is shown on the right.

2.2. Data Sets

2.2.1. Satellite Data

We have obtained four main data sets of satellite data in order to achieve for our analytical objectives. Two optical satellite data sets from the LANDSAT ETM+ with 30 m spatial resolution published by United States Geological Survey (USGS) and two microwave satellite data sets from the ALOS PALSAR published by Japan Aerospace Exploration Agency (JAXA). The selection of the optical satellite data were done by considering the following two critical issues. First, we had to choose a cloud free image for analysis. In fact, finding a cloud free scene is a general issue for all the researchers using optical satellite remote sensing images: clouds block the solar radiation from reaching the ground rendering the covered area unavailable for the observing platform. Second, the Scan Line Corrector (SLC) failure that occurred after May 31, 2003 makes the LANDSAT ETM+ line of sight tracing a zigzag pattern along the satellite ground track. As a result, imaged areas are duplicated, with widths increasing towards the scene edge (USGS, 2010). Although the ETM+ is continuing to acquire image data which are available for downloading at the USGS webpage, a gap fill has to be performed in order to correct the image to become usable for analysis. We needed to choose a winter season data for the purpose of our analysis. The data is preferable to choose the same year data, but because of the issue of the cloud cover this could not be fulfilled, and later year

data was chosen and because of that the issue of the gap fill needed to overcome. As a result, we selected the cloud free LANDSAT ETM+ image captured on May 25th, 2002 and Dec 30th, 2006 as the best fit for our analysis purposes.

For the microwave data, we have chosen the level 1.5 product of ALOS PALSAR L-band data of Sep 15th, 2009 and Oct 14th, 2009 for to cover the study area with an ascending Fine Beam Dual (FBD) Polarization, off nadir angle of 34.3 degree, 12.5 m ground range pixel spacing specification. A mosaic image of the study area is produced using these data sets.

2.2.2. Ground Truth

In order to verify the contents of the pixel on the images, we need to obtain a reference data to compare what is there in reality. Here, we have obtained three data to help determine the contents of the surface. One is The National Survey on the Natural Environment (6th and 7th Surveys, performed from 1999 and later on), which is published by the Ministry of Environment, Japan, provides the status of lands, surface waters and coastal areas all over the nation. The survey results are compiled and published in the form of written reports, maps, etc. The vegetation map so provided is utilized for identification of specific land-use/land-cover (LU/LC) sites for ground truth training data needed for land features classification and for the accuracy assessment of the classified images. Second, is the ALOS PRISM Panchromatic data with 2.5 m spatial resolution at nadir. This data is used with the combination of the vegetation map for the confirmation of the land surface. Third, a field observation was performed to collect ground truth data of the sites and identify the land features of the sites.

2.2.3. Digital Elevation Model (DEM)

A digital model of a terrains surface is obtained from the ASTER Global Digital Elevation Model (GDEM) with a spatial resolution of 30 m and an elevation accuracy of ±7 m published by the Earth Remote Sensing Data Analysis Center (ERSDAC). The data has been downloaded from the website and concatenated so that it covers the study area and could be used in the analysis.

3. Methodology

3.1. Satellite Remote Sensing

Remote sensing is a broad term. It's a technique for example, using satellites or aircrafts to observe various objects such as land, seas or atmosphere remotely. In satellite remote sensing, electromagnetic waves are used to remotely investigate the objects. Various electromagnetic waves which come from the solar radiation are being absorbed, transmitted or reflected by various objects on the earth. Spectral signatures differ among the objects and those signatures and the technique is used to investigate the status of the earth's surface. It can be described that, remote sensing is a technique to observe various objects without being in that certain location or taking direct contacts to it. The strength of satellite remote sensing is its range of spatial observation, and to observe the environment of any place around the world, even if you are not

there. It could also simplify the process of monitoring of the environment. The overall flowchart of the methodology of this research is presented in Figure.3.

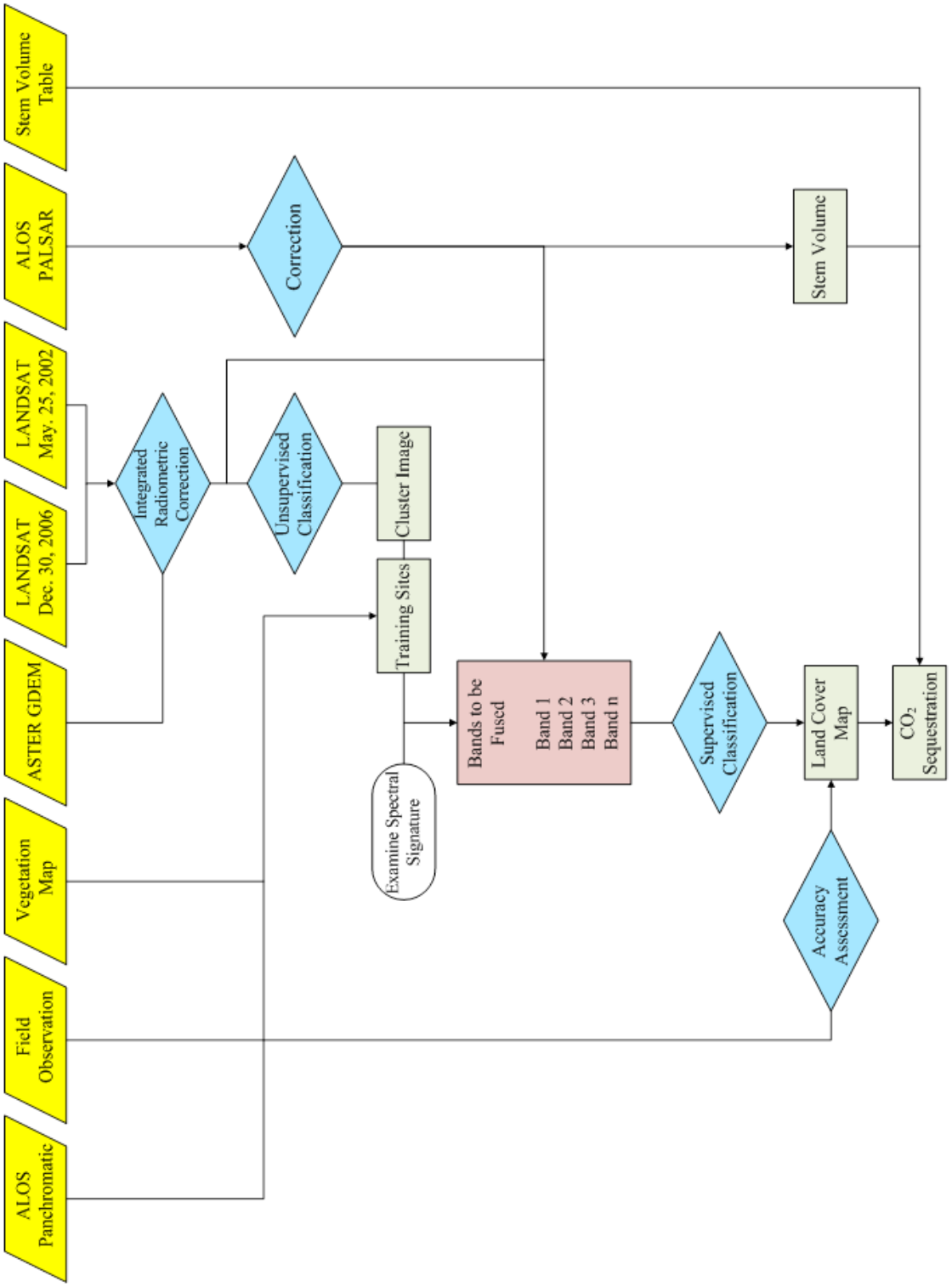

Figure 3. The analysis flowchart

3.1.1. GIS Software

In this research, the Clark Labs IDRISI Andes/IDRISI Taiga GIS platform was used for all the analysis. Various modules mounted and the high compatibility to other file format is the advantage of this software which will support our analysis. IDRISI Andes is the former version of IDRISI Taiga. Little changes in the interface and addition of new modules and supported file formats are the main differences although there are no minor changes in the calculations of the modules itself.

3.2. Gap Fill

As mentioned in section 2, the issue of the gap because of the SLC failure needs to overcome. Compared to the SLC-on data it can be seen that there are the gaps along the images on the SLC-off products (Figure.4 left). For the gap filling process, we used a frame and fill tool programmed by Richard Irish from NASA Goddard Space Flight Center. It uses the histogram matching method, calculating a transfer function which converts the radiometric values of one scene into equivalent radiometric values of a second scene, and then the transformed data are used to fill the gaps (USGS, 2004). After the gap filling process, the image can be seen with the gaps filled (Figure.4 right) and we assumed that this to be applicable for the analysis of the research.

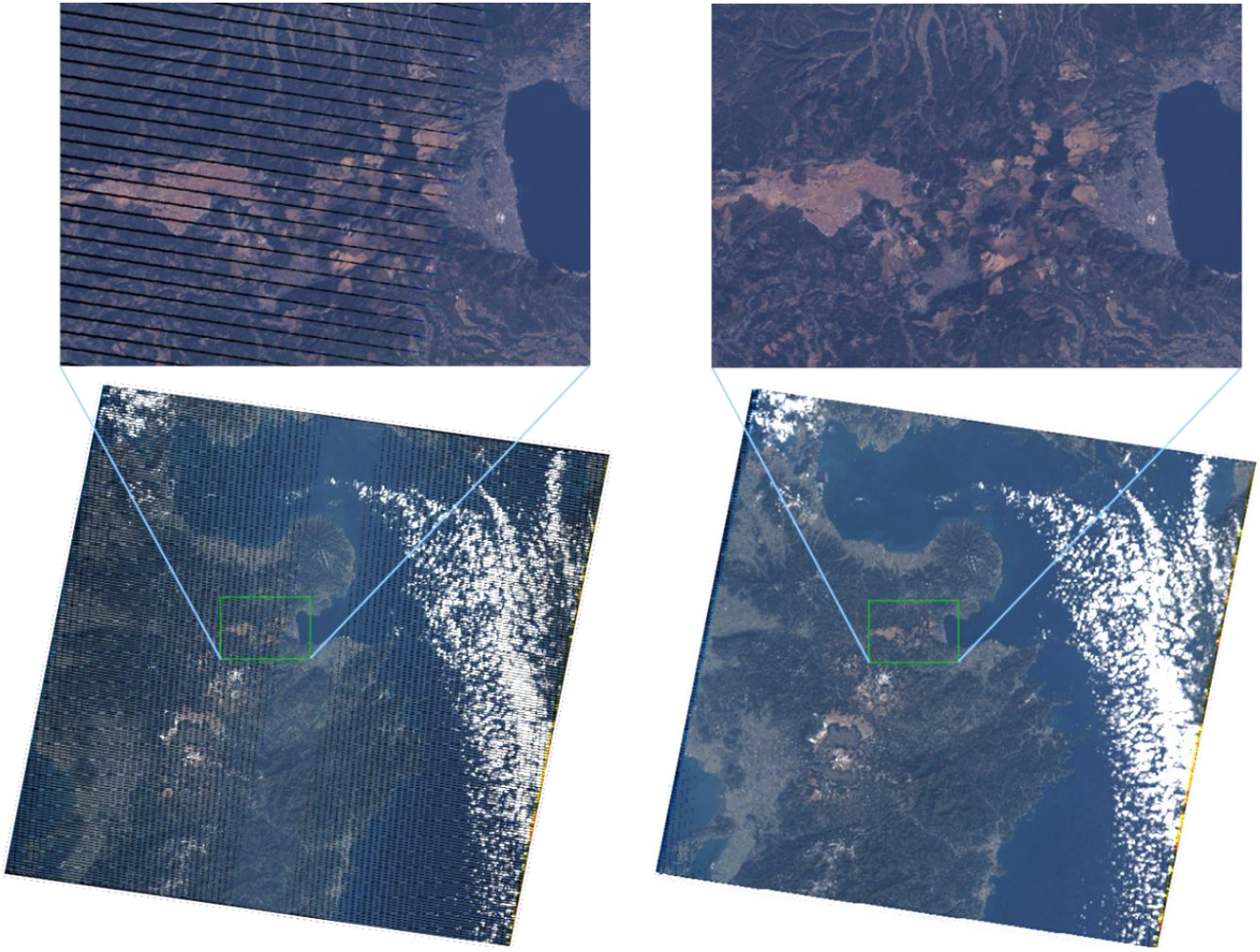

Figure 4. The LANDSAT ETM+ SLC-off product (Dec. 30, 2006). Performance of the gap fill, before (on the left) and after (on the right).

3.3. Radiometric Correction

Performing radiometric correction (atmospheric and topographic) to the remote sensing images is a crucial issue especially when dealing with such analysis that depends strongly on the information of the electromagnetic spectrum of the earth's objects. When the emitted or reflected electromagnetic energy is observed by a satellite sensor, the observed energy does not coincide with the energy emitted or reflected from the same object observed from a short distance. This is due to the solar azimuth and elevation, slope and aspects, atmospheric conditions such as haze or aerosols, etc. which influence the observed energy. Therefore, in order to obtain the actual irradiance or reflectance, those radiometric distortions must be corrected. For the correction of the images, we have applied the Integrated Radiometric Correction (IRC) method developed by Kobayashi & Sanga-Ngoie (2008). This method is a comprehensive radiometric calibration method aimed at simultaneous correction of atmospheric, solar, and topographic effects inherent to remote sensing data, which makes it possible to retrieve the at-surface reflectance and radiance values as if the atmosphere were totally transparent and the underlying surface was absolutely flat (Kobayashi & Sanga-Ngoie, 2008). The correction method follows with the atmospheric correction using the Dark Object Subtraction method and for the topographic correction, the derivation of solar and land geometric parameters, calculation of topographic correction factor, and atmospheric transmittance functions follows, then after retrieving these parameters we perform the IRC to fully correct the remote sensing imagery. The images were converted from Digital Numbers (DNs) to radiance values before entering the process.

Land geometric parameters can be derived from the DEM data. Using those parameters the cosine of the incidence angle (cos*i*) or the solar illumination and the h-factor which expresses the portion of the sky dome diffusing on to the tilted surface, can be given using equation (1) and (2):

$$\cos i = \cos\theta_z \cos e + \sin\theta_z \sin e \cos(\phi_e - \phi_s) \tag{1}$$

$$h = \frac{\pi - e}{\pi} = 1 - \frac{e}{\pi} \tag{2}$$

Where, θ_z is the solar zenith angle, e is the slope angle between the inclined surface and the horizontal plane, Φ_e and Φ_s represents the aspect angle of the inclined surface from the north and the solar azimuth angle from the north respectively.

Topographic correction factor (A-factor) is then calculated with equation (3):

$$\mathrm{A} = \frac{\cos\theta_z + Ch_0^{-1}}{\cos i + Ch_0^{-1}h} \tag{3}$$

Where, C is the parameter calculated as the quotient between the regressional intercept and slope of the expression between cos*i* and surface radiance as sensed by the satellite. h_0 is given by:

$$h_0 = \frac{\pi + 2\theta_z}{2\pi} \tag{4}$$

For the atmospheric transmittance functions, the Rayleigh scattering transmittance function (T_r) and water vapor transmittance function (T_w) was calculated. Expression (5) was used for the Rayleigh scattering transmittance ($T_{r\lambda}$) as a function of wavelength (λ), the ambient atmospheric pressure (P) and the sea level atmospheric pressure (P_0) in mbar.

$$T_{r\lambda} = \exp\left(-\frac{P}{P_0} \times M \times \frac{1}{115.6406\lambda^4 - 1.335\lambda^2}\right) \quad (5)$$

Where M is the relative air mass expressed as:

$$M = \frac{1}{\cos\theta_z + 0.15(93.885 - \theta_z)^{-1.253}} \quad (6)$$

For the atmospheric pressure (P) we did not assume $P \approx P_0$ as the author did since the elevation of the study area varied up to 1758 m at the highest, so instead we have used equation (7) to calculate the atmospheric pressure for each pixel locations.

$$P = P_0 \exp\left(-\frac{a_i}{a_0}\right) \quad (7)$$

Where, a_i is the altitude at a certain pixel and a_0 is the scale height. We have assumed the scale height to be 7900 m so that the model could match with the standard pressure described as a function of altitude by Holton (1992).

The water vapor transmittance function is a function of water vapor absorption coefficients ($a_{w\lambda}$), relative air mass (M) and precipitable water vapor (W) measured in centimeters. Given as:

$$T_{w\lambda} = \exp\left[-\frac{0.2385\alpha_{w\lambda}WM}{(1 + 20.07\alpha_{w\lambda}WM)^{0.45}}\right] \quad (8)$$

For the precipitable water vapor, we could not get the spatial data so we have determined here W to be a constant value.

With all the parameters calculated the expression for IRC yields finally:

$$L_g = (L_s^* - L_h)\frac{A}{0.5(1 + T_r)T_rT_w^2} \quad (9)$$

Where, L_g is the corrected radiance from the surface, L_s^* is the at-satellite observed spectral radiance from a sloped terrain and L_h is the upwelling atmospheric spectral radiance. All the optical data of 2002 and 2006 data from band 1 to 5 and band 7 was corrected through this process.

3.4. Vegetation Map

Producing a land cover map (detailed vegetation map) is one of the main objectives to achieve the goal for this research. The land cover map contains important information of what (urban, forest, water bodies etc.) is where and how much there are, and this map will be one of the source for the estimation of CO_2 sequestration. The land cover map will be produced using the satellite remote sensing imagery. The year 2002 data will be the main data for the analysis

while the year 2006 data and the PALSAR data will be a supplemental data for adding more information to the classification process for producing detailed land cover map.

3.4.1. Hybrid Classification

We have downloaded the polygon data of the administrative district published by the National and Regional Planning Bureau of Ministry of Land, Infrastructure, Transport and Tourism (MLIT). The polygon data of Oita prefecture is converted to a raster format Boolean image, and overlayed with the LANDSAT ETM+ image to extract the area of Oita Prefecture. All the bands from band 1 to band 7 (except band 6) are processed and for the PALSAR image too. The PALSAR image has been resampled to 30 m resolution using bilinear method to match with the LANDSAT imagery. The classification process for producing the land cover map will be based on this extracted imagery.

The Hybrid Classification method (Richards & Jia, 1999; Sanga-Ngoie & Kobayashi, 2003) is implemented for the classification process. This method uses both the unsupervised classification and supervised classification (Richards & Jia, 1999; Kato, 2004; Eastman, 2006), with the former classification first and on the base of the cluster image, which was produced by the unsupervised classification ISOCLUSTER module, the training site will be created and used in the supervised classification process. In the case of supervised classification, the software system delineates specific land cover types based on statistical characterization data drawn from known examples in the image (known as training sites). This "training sites" will be taken for each information classes (i.e. land cover types) and that information is then used to develop statistical characterization of reflectance/radiances for each information class as simple as the mean or the range of reflectance/radiances on each band, or as complex as detailed analyses of the mean, variances and covariances over all bands (Eastman, 2006). To verify the land cover type on the cluster image, the vegetation map published by the Ministry of Environment, Panchromatic data, and the information observed from the sites were utilized. The advantage of the hybrid classification is that when only supervised classification is implemented, its major drawback lies in the need to have delineated unimodal spectral classes beforehand, which by using unsupervised classification, this can be handled.

3.4.2. Maximum Likelihood

In the supervised classification, there are various methods for making decision about which pixel belongs to what classes. Parallelepiped, minimum distance to means, maximum likelihood, decision tree, linear discriminant analysis, etc. all of these methods differ only in the manner in which they develop and use statistical characterization of the training site data. In our analysis, the maximum likelihood method is used since this method estimates the posterior probability that a pixel belongs to each class, in other words, it gives the pixels to the most likely class based on the mean and variance/covariance data of the signatures from the training sites. This method is also the most widely used classifier in the classification of remotely sensed imagery. The spectral signature of each classes were examined through different bands to consider which bands will be used for the classification, while various

combinations of bands were experimented for checking which output gives the most reliable result. The images used for the classification is all radiometric corrected including the PALSAR data. The correction for the PALSAR data is described in section 3.6.2.2.

3.5. Accuracy Assessment

After the process of classification for producing land cover maps, accuracy assessment is an obligating process for evaluating the accuracy or the reliability of the map produced. The polygon data of the vegetation map published by the Ministry of Environment (Figure.5) was used assuming this as a ground truth, and the accuracy of the land cover map will be based on this information. Multiple sample points (over 29000) were generated using the stratified random sampling on the vegetation map to collect the ground truth points of the study area. Using this ground truth points and the land cover map, the accuracy will be assessed.

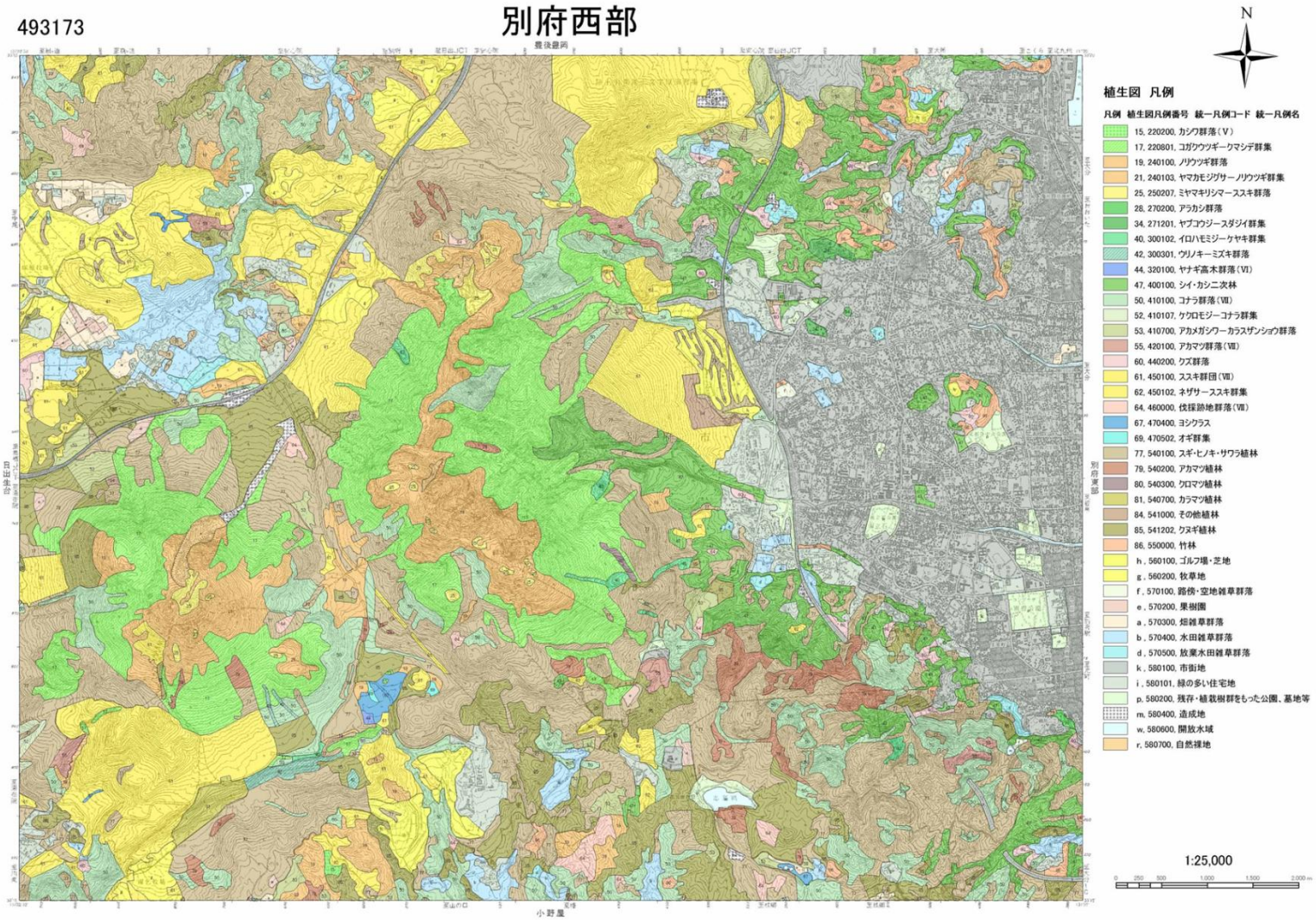

published by the Ministry of Environment. Part of a region at the study area.

3.5.1. Conventional Error Matrix

The ERRMAT module outputs the error matrix representing which classes matched the referenced classes, with the overall accuracy, omission and commission errors, and also outputs the information of Kappa Index of Agreement (KIA), and confidence interval. The Kappa value (K) can be calculated by equation (10)

$$\mathrm{K} = \frac{P_0 - P_\mathrm{c}}{1 - P_\mathrm{c}} \tag{10}$$

Where P_0 is the observed accuracy (proportion of agreeing units) and P_C is the chance agreement (proportion of units for expected chance agreement). For the per-category Kappa ($\mathrm{K_i}$) IDRISI follows the algorithm introduced to remote sensing by Rosenfield and Fitzpatrick-lins (1986):

$$\mathrm{K_i} = \frac{P_\mathrm{ii} - P_\mathrm{i+}P_\mathrm{+i}}{P_\mathrm{i+} - P_\mathrm{i+}P_\mathrm{+i}} \tag{11}$$

Where $\mathrm{P_{ii}}$ is the proportion of units agreeing in row i / column i and $\mathrm{P_{i+}}$ is the proportion of units for expected chance agreement in row i, and $\mathrm{P_{+i}}$ is the proportion of units for expected chance agreement in column i.

3.5.2. Fuzzy Accuracy Assessment - Fuzzy Error Matrix

Fuzzy Accuracy Assessment is a concept that to focus more on the complexity of the environment and reflecting that in the accuracy assessment procedure. Gopal and Woodcock (1994) proposed the use of fuzzy sets to "allow for explicit recognition of the possibility that ambiguity might exist regarding the appropriate map label for some locations on the map. The situation of one category being exactly right and all other categories being equally and exactly wrong often does not exist." It is recognized that instead of a simple system of correct and incorrect, there can be a variety of responses such as "absolutely right", "good answer", "acceptable", "understandable but wrong", and "absolutely wrong". Green and Congalton (2004) introduced the technique called the fuzzy error matrix approach also stated by Congalton and Green (2009), which is a technique using the error matrix computed from the conventional accuracy assessment. It takes the process of generating a fuzzy error matrix from a set of fuzzy rules applied to the same classification that was used to generate the conventional error matrix. In the matrix it will not show just the correct or incorrect results, rather instead they will change this to accept or poor results. The categories which are in the category of accepted will be counted as a matched result while the poor will be considered as an error. Here we will implement this fuzzy accuracy assessment to reflect the reality (heterogeneity) of the environment in the accuracy assessment. The overall flowchart for this method is presented in Figure.6.

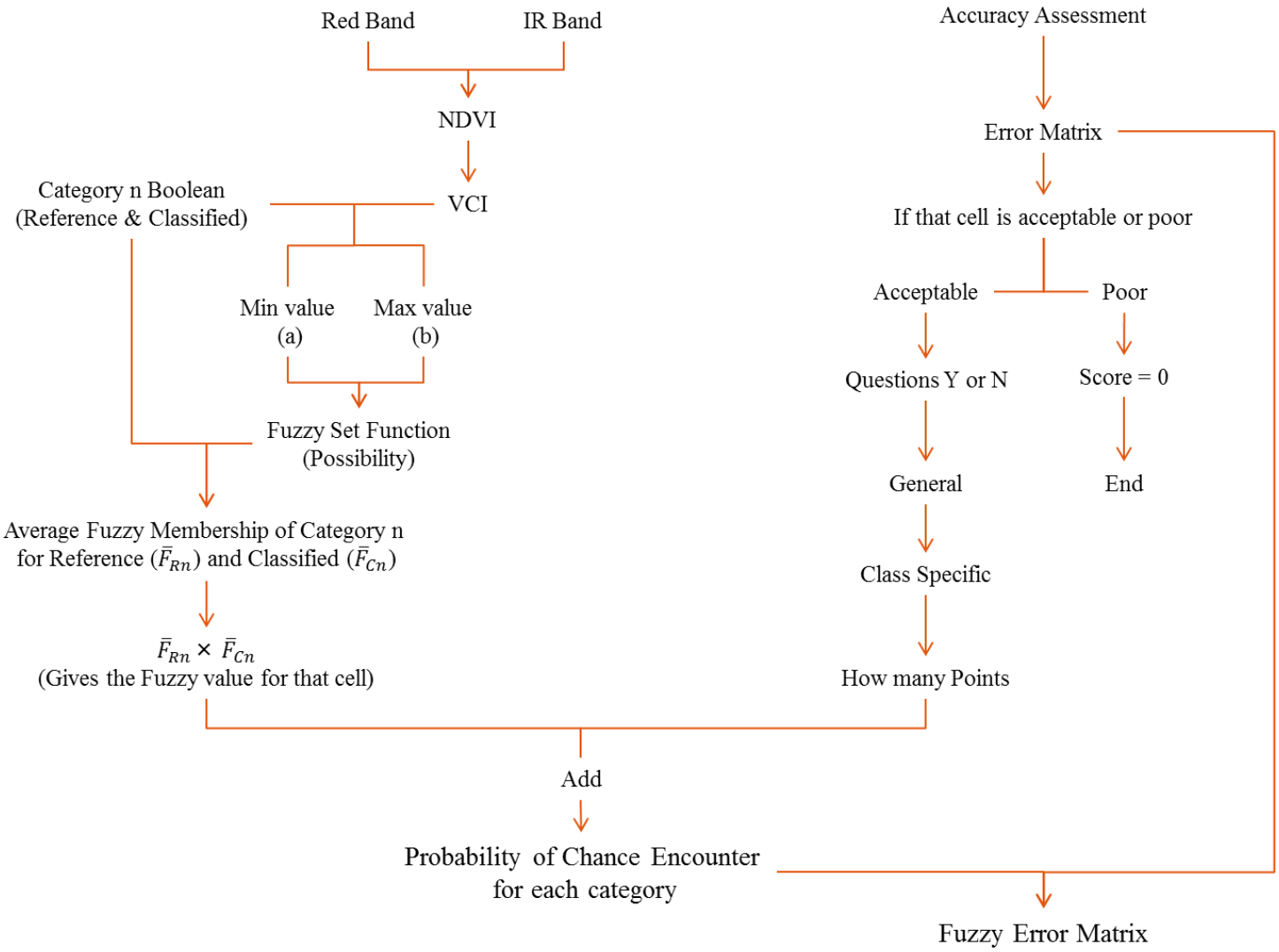

Figure 6. Overall flowchart of the fuzzy accuracy assessment to modify the conventional error matrix to the fuzzy error matrix.

First, a set of questions (Table.1) are prepared for to answer which will be a weighting factor for the final assessment. The questions are based on the information of physical explanation or interpreters' variability which could lead to an error of the land cover map. Each question is given weights so that according to the answer chosen, each category will be given that score. The questions will be answered for each cell in the matrix (the category where the reference and the classified class meets), although the cells to be answering the questions will be based on if that class is accepted to go through this procedure or not. If is considered as accepted, the procedure continues while if it is poor, that cell on the matrix will be ignored. The decision on if that cell is accepted or not depends on if the confusions between those classes could actually lead to the misclassification of the land cover (i.e. coniferous and evergreen forests), and if there is no way of getting misclassified it will be considered as poor (i.e. residential areas and water bodies).

Table 1. The questions of the weighting factors. The questions are separated into two, one is the general and the other is the class specific. The general has the general issues which would lead to an error as a general thing, while the class specific will gives questions that focus on each land features.

General	Scores for answer		
Is the satellite image corrected (atmospheric/topographic)	Y = 1		N = 0
Is there a limitation in the reference data collection method/Is the reference data reliability uncertain	Y = 1		N = 0
Is the interpreter variability controlled	Y = 0		N = 1
Class Specific			
Is the spectral signature of the class difficult to differentiate with the mapped class	Y = 2	Little difficult = 1	N = 0
Is the class more dominant than the mapped class	Y = 1		N = 0
Does the class change its scenery in a annual period of time	Y = 1		N = 0
Is the mapped class ecosystem highly heterogeneous	Y = 2	To some extent = 1	N = 0

Second, Vegetation Condition Index (VCI) (Kogan, 1998) will be used for the fuzzy set function computing the fuzzy membership (possibility) of each category. VCI can be calculated from the equation below:

$$\mathrm{VCI} = \frac{\mathrm{NDVI_i} - \mathrm{NDVI_{min}}}{\mathrm{NDVI_{max}} - \mathrm{NDVI_{min}}} \tag{12}$$

Where, $NDVI_i$ is the NDVI value at a certain pixel, $NDVI_{min}$ is the minimum value of the NDVI and $NDVI_{max}$ is the maximum value of the NDVI. The Normalized Difference Vegetation Index (NDVI) can be calculated from the remote sensing imagery with the below equation:

$$\mathrm{NDVI} = \frac{\mathrm{IR} - \mathrm{R}}{\mathrm{IR} + \mathrm{R}} \tag{13}$$

Where, IR represents the infrared band of the satellite imagery and R for the red band imagery. NDVI is an indicator which can be used to analyze the activity of the vegetated areas. The value takes the range from -1 to 1 meaning that there are more activeness when the value becomes 1. This can be understood by the mechanism that the chlorophyll in the leaves has a character of reflecting the near infrared wavelength and absorbing more in the red wavelength, so by calculating this we can detect which area that has more greenness on the surface.

This possibility from the VCI will be added with the weighting factor from the questions and used for the calculation in the error matrix to decide the number of points (ground truth points) in each category, to be in the accepted or the poor.

3.6. Estimation of CO_2 Sequestration

3.6.1. Estimation using Averaged Sequestration Value

Using the information of the total forest area derived from the land cover map, the estimation of the sequestration will be done by using the averaged sequestration values of each forest types observed by Tadaki and Hachiya (1968). Multiplying the total forest area by the averaged value per unit area will give us the results of the total sequestration value of each forest types. The sequestration value is the aboveground Net Primary Product (NPP), which is the value of the CO_2 absorbed from the photosynthesis process subtracting the respiration activity (Matsumoto, 2001).

3.6.2. Estimation Considering Tree Age

Not only with the simple estimation for each forest types, but the estimation considering tree ages were examined. This is due to the differences in the sequestration rate among different tree ages, so by considering the sequestration per tree age, it would be a more precise estimation rather than using only the averaged sequestration value. Therefore we have estimated the tree ages based on two methods, one is using the optical data computing NDVI and using that to classify the ages of the forests, and second is using the microwave data to classify the forest area into tree ages categories.

3.6.2.1. Classifying Tree Age based on NDVI

The relationship between NDVI and tree age was deduced by Ishii (2007) based on the Forest Tree Age growth curve and multi-temporal NDVI data (Figure.7).

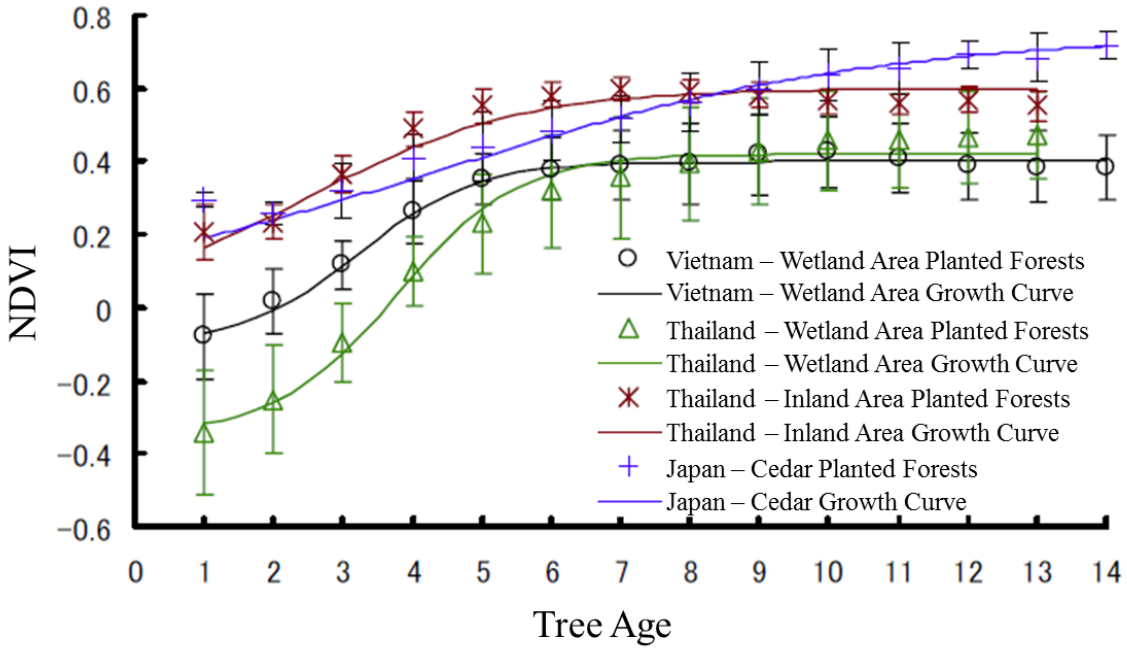

Figure 7. Forest Tree Age growth curves (Ishii, 2007). Different forest types in multiple locations from Vietnam, Thailand and Japan. The blue line shows the Japanese Sugi (Cedar) Forests growth curve.

Referring to this growth curve, we could thus classify the coniferous forests area into separate tree ages categories. The classification of the tree ages was implemented only to the coniferous (cedar) forests by using this method, since the relation between the NDVI and forest tree age growth was analyzed with that type of forests.

3.6.2.2. Classifying Tree Age based on Stem Volume

The PALSAR data was used for the analysis of stem volume, so that the tree ages can be known. The DN values were converted to the backscattering intensity (σ^0) in decibel units using equation (12)

$$\sigma^0 = 10\log_{10}\mathrm{DN}^2+\mathrm{CF} \qquad (14)$$

CF is the calibration factor for the PALSAR product, for the level 1.5 product CF=-83.0 dB. For a correct interpretation of the backscatter signatures, corrections for the effect of local incidence angle and normalization for the true pixel area were necessary.

The corrected backscatter in gamma nought (γ^0) format can be obtained from the sigma nought (σ^0) value according to Castel et.al (2001) and Ulander (1996), which has also been applied by other authors (Chen et.al, 2009; Santoro et.al, 2009; Armston et.al, 2010; Santoro et.al, 2011).

$$\gamma^0 = \sigma^0 \frac{A_{flat}}{A_{slope}} \left(\frac{\cos \theta_{ref}}{\cos \theta_{loc}} \right)^n \quad (15)$$

Where, θ_{loc} and θ_{ref} represents the local incidence angle and a reference angle for the normalization of the backscatter (e.g. off nadir angle) respectively. A_{slope} and A_{flat} represents the true pixel area and the local pixel area for a theoretically flat terrain respectively. For details refer to Castel et.al (2001) and Ulander (1996). For bare surfaces, the exponent *n* is equal to one. For vegetated surfaces, it expresses the variation of the scattering mechanism due to the presence of a volume on the sloped terrain, thus being related to the optical depth of the vegetation. At the forest site of Lozere, France, the value was estimated lower and equal to 0.36 for the Japanese Earth Resources Satellite (JERS)-1 L-band SAR backscatter. The lack of detailed information about optical depth of the forest canopies at the study area was determined but we have applied the 0.36 value since that the scattering properties of the forests should be taken into account. For future works, this should be reconsidered for the case of different polarizations also. In the case of γ^0, as opposed to the case of σ^0 or β^0, the unit area is taken perpendicular to the axis of the radar beam.

The relationship between backscattering intensity and stem volume or biomass has been analyzed by various researchers (Kuplich et.al, 2000; Champion et.al. 2008; Karjalainen et.al 2008; Chen et.al, 2009; Wijaya, 2009; Santoro et.al, 2011). Through various studies, it is stated that the backscattering signature correlates with the forest parameters, and it has been shown in many studies that SAR images can be used to extract forest biomass related information. Because of time, we did not have a chance of collecting ground data of the stem volume in our study area, so we have implemented the polynomial model developed by Wijaya (2009) (equation (14)) to estimate the stem volume.

$$V = 256.85 - (65.458\sigma) - (6.8\sigma^2) \quad (16)$$

Where, *V* is the stem volume and σ is the backscattering intensity. The reason we used this model was because the data they have used was the most similar data compared to our data (PALSAR L-band FBD 34.3˚ HH/HV specifications). The stem volume map produced using this model was then classified into ages among the forests referring to the relationship of the tree age and stem volume information provided by Oita Prefectural Government. The classification was done to the coniferous and deciduous broad leaf forests but not the evergreen broad leaf forests because there were no data for that forest type. The data of Sugi (Cedar) and Saw Tooth Oak was used as the coniferous forests and deciduous broad leaf forests respectively.

4. Results

4.1. Evaluation of Radiometric Correction

Before performing the IRC, the remote sensing images were needed to be corrected for atmospheric effects. The Dark Object Subtraction method was implemented and the radiance value was computed for all the bands for correction (Table.2) and as you can see the

remarkable decrease in the haze value with the increasing of wavelengths. This haze value was subtracted by the whole pixel values on the image.

Table 2. Computed haze values: L_h (measured in $Wm^{-2}\,\mu m^{-1}\,sr^{-1}$).

	Band 1	Band 2	Band 3	Band 4	Band 5	Band 7
May	40	11.8	5	1.3	0.13	0.05
Dec	26	11.8	5	1.3	0.13	0.04

After the atmospheric correction, the IRC is performed. Quantitative evaluation of the performance of the correction is done by assessing the non-correlationship between the solar illumination (cos*i*) and the corrected data. In Figure.8, it shows the regression analysis between the solar illumination and non-corrected data on the left, which can be seen with a high correlation, with higher radiance for higher cos*i* value because of topographic effects. However, in the same Figure.8 on the right, the correlation between those two can be seen with lower or mostly non correlation which is the data after the correction. Figure.9 shows the example of the difference of images before the correction and after for band 4. The zoomed area is a mountainous location and the radiance values are corrected in those areas, while the areas on the top left side can be seen without the changes where it is the residential areas.

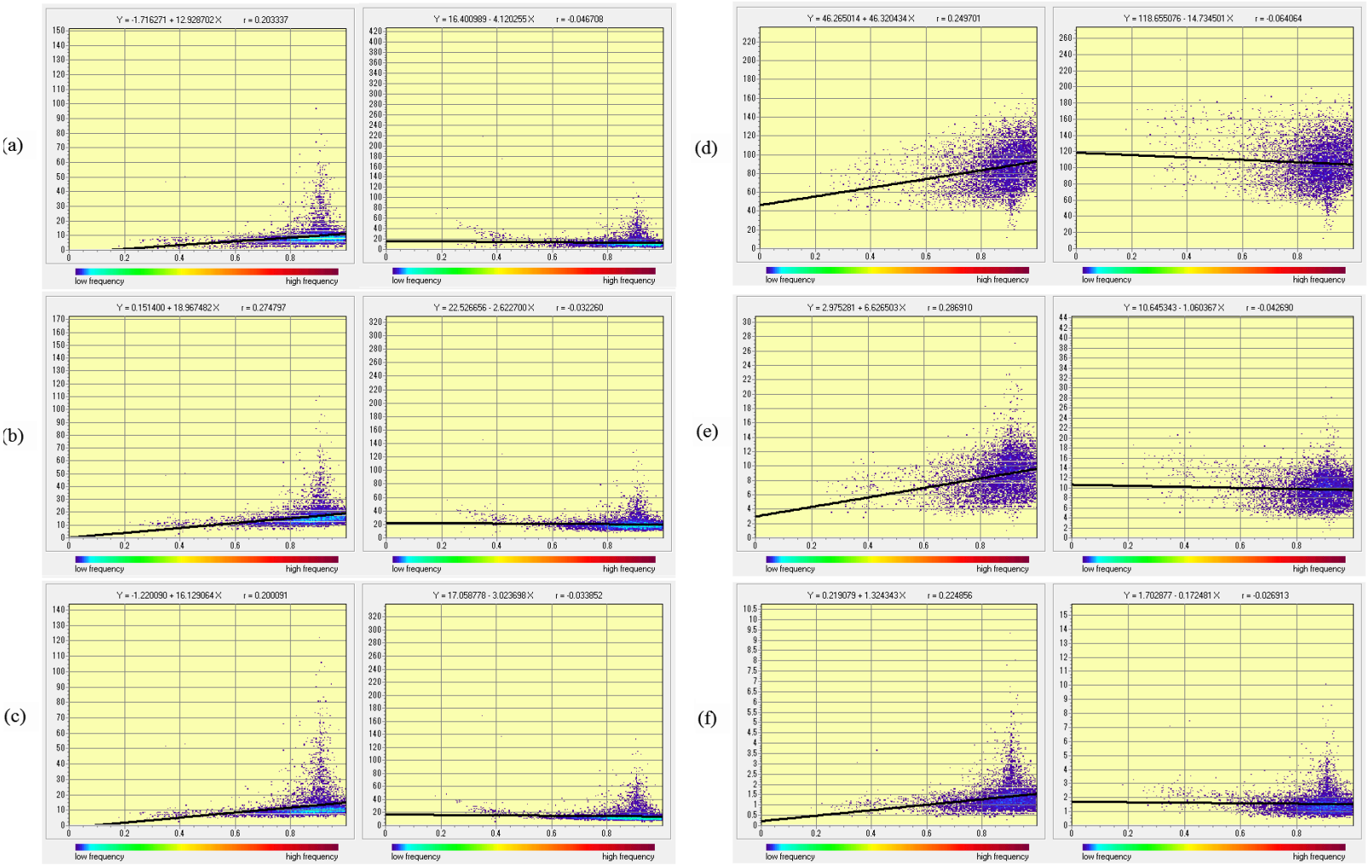

Figure 8. Regression analysis between the solar illumination (cos i) as x-axis, and the radiance value as y-axis for (a) band 1 (b) band 2(c) band 3(d) band 4(e) band 5 and (f) band 7.

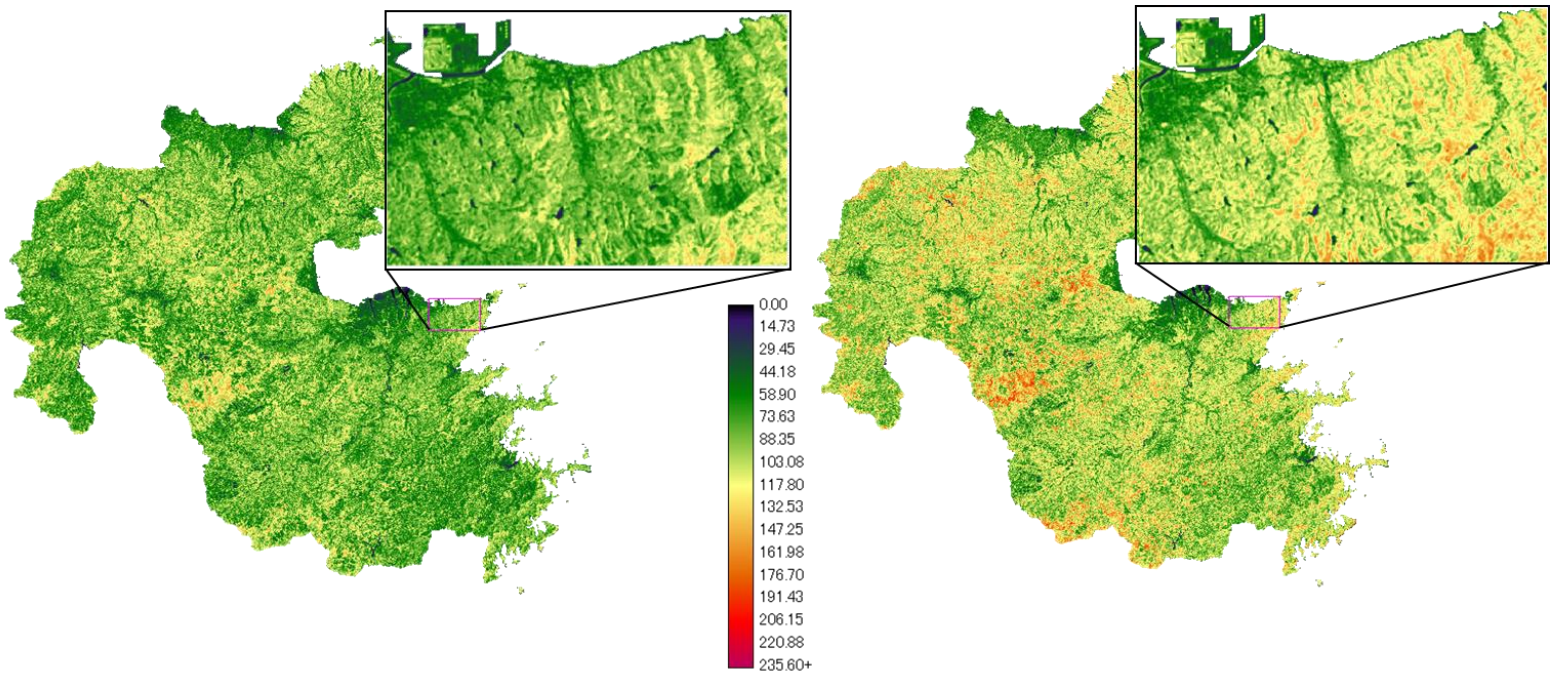

Figure 9. Original near-infrared band (band 4) image (left) and IRC corrected image (right) in radiance over the study area.

4.2. Land Cover Map - Vegetation Map

4.2.1. Extracting Oita Prefecture

Using the polygon data of the administrative district, it has been overlayed with the LANDSAT and PALSAR images for each bands and polarization to extract the study area (Figure.10). This area will be the area for the analysis and the images will be the bases for the analysis of unsupervised and supervised classification.

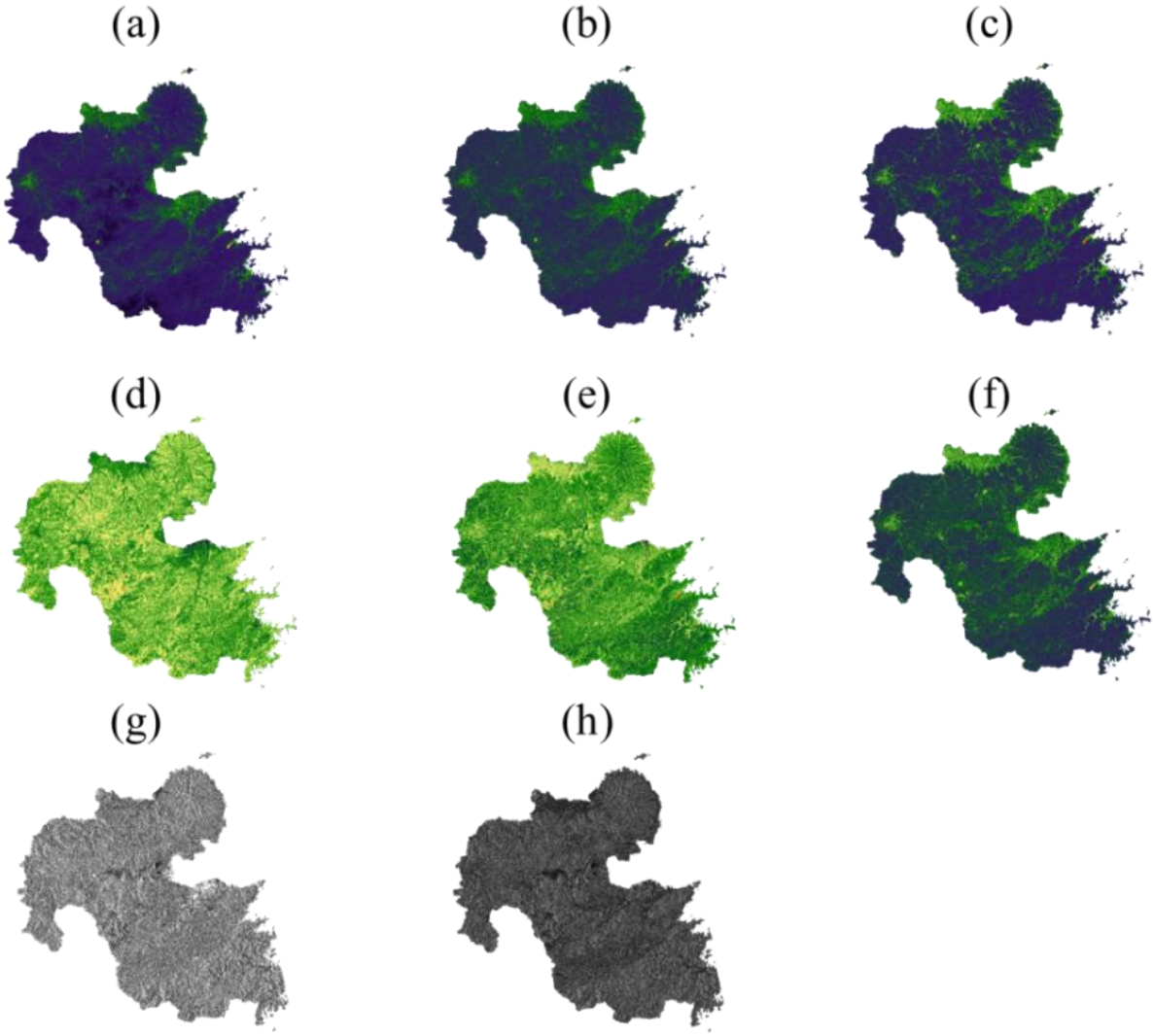

Figure 10. Extraction of Oita Prefecture for LANDSAT ETM+ (a) band 1 (b) band 2 (c) band 3 (d) band 4 (e) band 5 (f) band 7 and PALSAR (g) HH (h) HV.

4.2.2. Unsupervised Classification

Using the images which the study area was extracted, the unsupervised classification ISOCLUSTER module was performed to produce a cluster image (Figure.11). Corrected images band 1 to 5 and NDVI data was used with 100 times iterations outputting 20 classes.

On this image, you can see the cluster of each classes but not identified as what land cover it is corresponding to. The training sites will be constructed on the top of this cluster image so it can be handled easier for where the class border changes. The constructed training sites will be used in the latter supervised classification process.

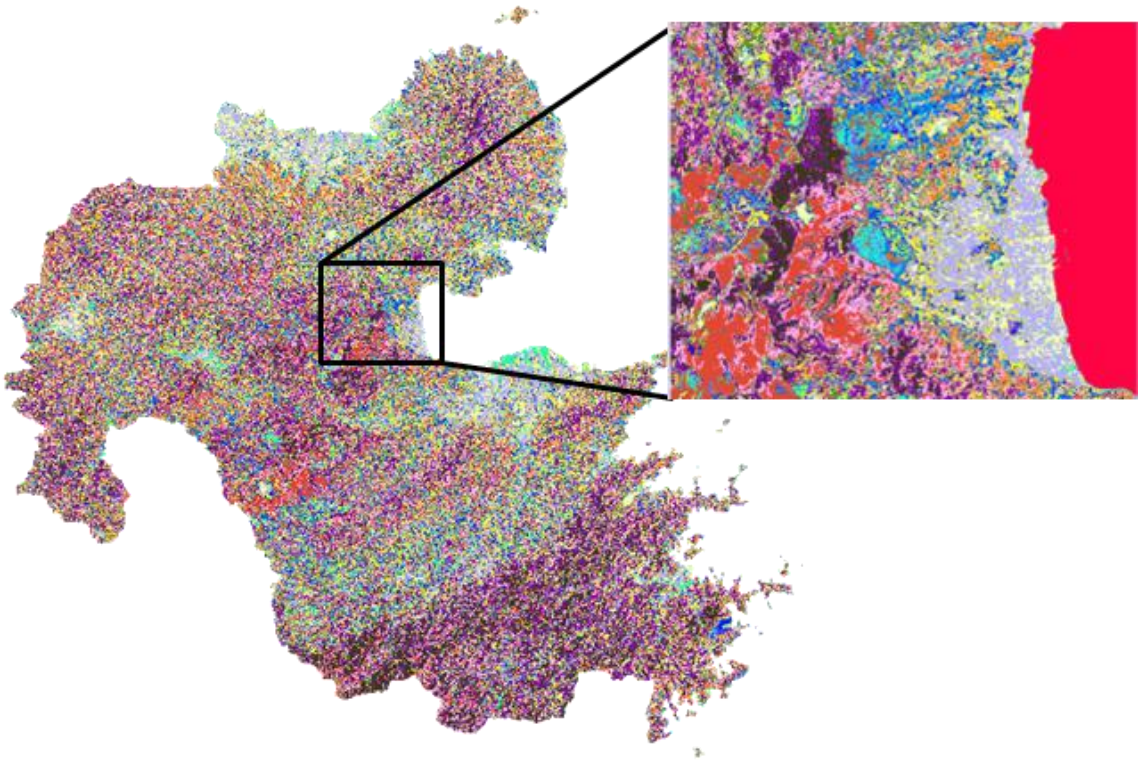

Figure 11. Cluster image produced by the ISOCLUSTER module.

4.2.3. Supervised Classification

Comparing with the supervised classification alone, the process of constructing the training sites are more accurate and it will result with higher accuracy of the land cover map due to the precise information of the spectral signature of that certain land cover type.

Figure.12 shows the spectral signature of each land cover types along different bands of LANDSAT ETM+. The y-axis is the radiance unit and the values for each class are represented with the mean radiance of the pixels taken by the training sites. Similarity can be seen among some classes (e.g. forests) although totally different spectral signature can be seen in some other classes (e.g. residential area and water bodies). This spectral difference is the characteristics of those classes for to differentiate with other classes.

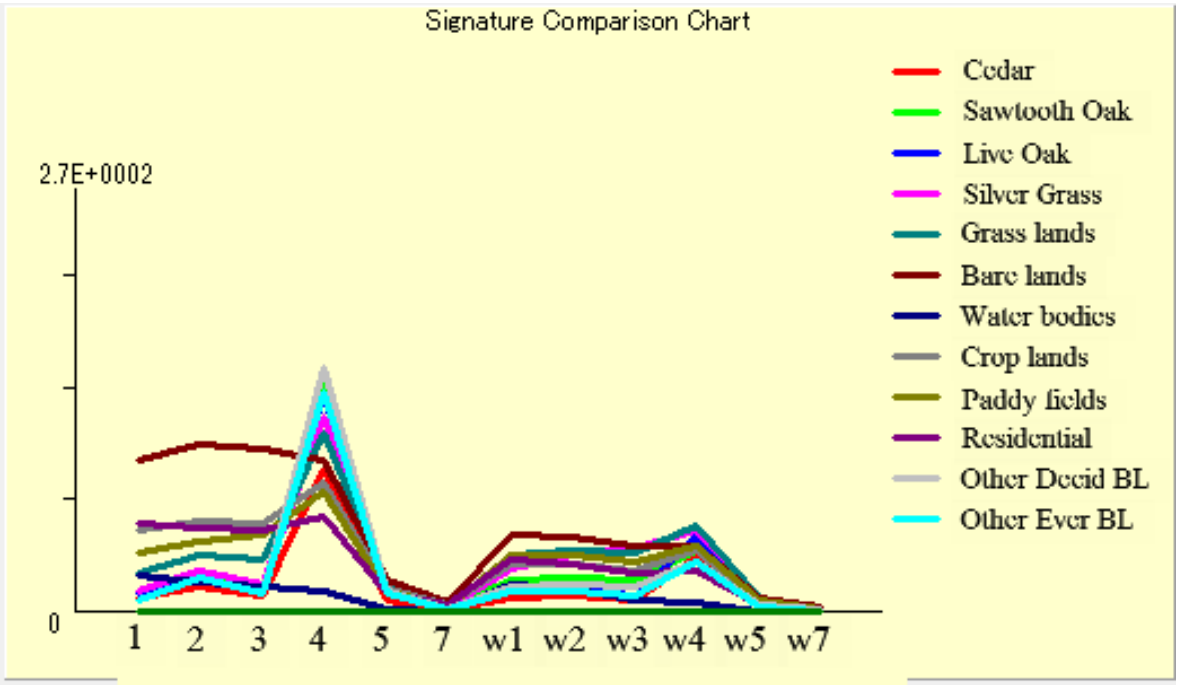

Figure 12. Signature comparison between land cover types. It is the mean radiance value taken from the pixels where the training sites were constructed. 1 to 7 is the May data mean value from band 1 to 7, while w1 to w7 is the December data mean value from band 1 to 7.

4.2.4. Maximum Likelihood

MAXLIKE module uses the spectral signature of the classes with the images to be fused, and the pixels will be classed to the most likely classes they would belong according to the algorithm. The final product of the land cover map is shown in Figure.13 which is the reclassified map from the original 12 classes to 10 classes. The category of 12 classes and the 10 classes are shown on Table.3 with which class was merged to what class. This product was chosen from the various outputs made by using various bands of satellite images to see the differences of accuracies among them all shown on Table.4. May and Dec represents which month data sets were used in the process, while $NDVI_{May}$ is the NDVI data from the May data and $NDVI_{Dec}$ is the data from December. HV is the PALSAR HV polarized backscattering data and the correct and no correct is if the images were radiometric corrected or not.

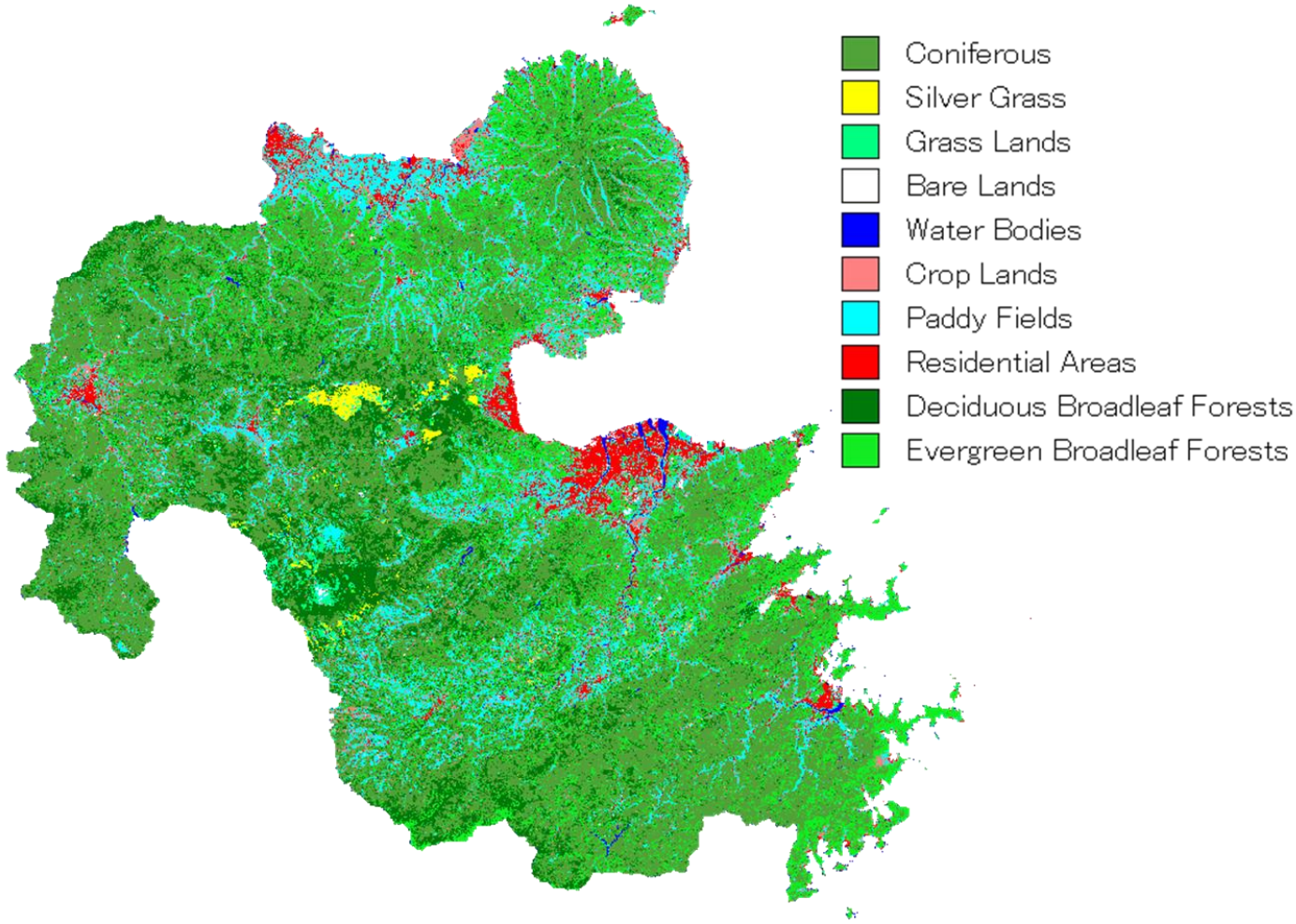

Figure 13. The final output of the land cover map.

Table 3. Land cover classes. Left = Original output; Right = Final product.

Class 1	Cedar-Cypress (*Sugi-Hinoki*)	Class 1	Coniferous Forests
Class 2	Saw Tooth Oak (*Kunugi*)	Class 2	Silver Grass (*Susuki*)
Class 3	Live Oak (*Shii-Kashi*)	Class 3	Grass Lands
Class 4	Silver Grass (*Susuki*)	Class 4	Bare Lands
Class 5	Grass Lands	Class 5	Water Bodies
Class 6	Bare Lands	Class 6	Crop Lands
Class 7	Water Bodies	Class 7	Paddy Fields
Class 8	Crop Lands	Class 8	Residential Areas
Class 9	Paddy Fields	Class 9	Deciduous BL Forests
Class 10	Residential Areas	Class 10	Evergreen BL Forests
Class 11	Deciduous BL Forests		
Class 12	Evergreen BL Forests		

Table 4. Accuracy of the land cover map from the classification process, on the combination of multiple images with Type A = 12 class and Type B = 10 class.

Used Image	Type	Accuracy %
No Corrected May	A	47.3
No Corrected May	B	51.5
Corrected May	A	51.3
Corrected May	B	54.6
Corrected May + $NDVI_{May}$	A	51.5
Corrected May + $NDVI_{May}$	B	55
Corrected May + HV	A	51.9
Corrected May + HV	B	55.1
Corrected May + $NDVI_{May}$ + HV	A	51
Corrected May + $NDVI_{May}$ + HV	B	54.5
Corrected May + Corrected Dec	A	52.4
Corrected May + Corrected Dec	B	55.2
Corrected May + Corrected Dec + $NDVI_{May}$ + $NDVI_{Dec}$	A	52.7
Corrected May + Corrected Dec + $NDVI_{May}$ + $NDVI_{Dec}$	B	55.5

4.3. Accuracy Assessment

4.3.1 Conventional Error Matrix

The ground truth points obtained from the reference data was used with the land cover map to perform the accuracy assessment by outputting the error matrix (Table.5).

Table 5. Error Matrix showing the reference data versus the image classification.

Classified \ Reference	Coniferous	Silver Grass	Grasslands	Bare lands	Water bodies	Crop lands	Paddy fields	Residential	Deciduous-Bl	Evergreen-Bl	Total	ErrorC	Users A
Coniferous	**9305**	100	52	16	61	125	158	39	1086	1543	12485	25.47%	74.53%
Silver Grass	6	**365**	48	7	2	7	3	1	17	0	456	19.96%	80.04%
Grasslands	69	192	**211**	17	8	86	71	26	65	18	763	72.35%	27.65%
Bare lands	5	10	14	**41**	12	5	7	59	3	2	158	74.05%	25.95%
Water bodies	5	9	2	12	**279**	0	8	6	1	14	336	16.96%	83.04%
Crop lands	179	29	67	52	28	**235**	237	197	42	71	1137	79.33%	20.67%
Paddy fields	309	128	129	109	223	216	**1339**	349	120	105	3027	55.76%	44.24%
Residential	5	15	40	55	70	34	104	**651**	7	9	990	34.24%	65.76%
Deciduous-Bl	1190	363	129	18	4	85	73	12	**1788**	500	4162	57.04%	42.96%
Evergreen-Bl	1734	77	89	25	16	257	108	44	1123	**1729**	5202	66.76%	33.24%
Total	12807	1288	781	352	703	1050	2108	1384	4252	3991	**28716**		
ErrorO	27.34%	71.66%	72.95%	88.35%	60.31%	77.62%	36.48%	52.91%	57.95%	56.68%		44.48%	Overall Accuracy
Producers A	72.66%	28.34%	27.02%	11.65%	39.69%	22.38%	63.52%	47.04%	42.05%	43.32%			15943/28716 = 55.52%

Here, the reference data (ground truth) is presented in the column and the classified category is in the row. Major diagonal of the error matrix represents agreement between the reference data and the classified map, and is represented by a single cell in the matrix for each map class. It is computed with the user's accuracy (Error of Commission) for the row total and the producer's accuracy (Error of Omission) for the column total. The overall accuracy is considered with sum of the points which has the exact match between the reference data and the classified data (major diagonal in bold) divided by the total number of points. The overall accuracy of the land cover map resulted at 55.5 % which was produced using the May and December data with the NDVI data of both months.

4.3.2. Fuzzy Error Matrix

Now on the base of this error matrix, the fuzzy error matrix is developed. But, to consider how many points that will be considered as the accepted or poor will be determined by the method developed here. Table.6 shows the total scores for each category based on the set of questions from Table.1.

Table 6. The scores per category for the accepted classes from the questions.

		Reference									
		Coniferous	Silver Grass	Grasslands	Bare lands	Water bodies	Crop lands	Paddy fields	Residential	Deciduous-Bl	Evergreen-Bl
Classified	Coniferous	-								5	5
	Silver Grass		-	5			5				
	Grasslands		5	-			5	5			
	Bare lands				-			5	4		
	Water bodies					-		4			
	Crop lands		7	6			-	8	9		
	Paddy fields		7	7	7	6	8	-	8		
	Residential				4		6	6	-		
	Deciduous-Bl	7								-	8
	Evergreen-Bl	6								8	-

The VCI is calculated by the NDVI and it will be used in the process for computing the degree of possibility for each category by using the fuzzy set membership function. The minimum and the maximum value of the VCI are checked for each land cover classes of the classified data and the reference data. Each minimum and the maximum VCI values are used as the inflection points for the sigmoidal membership function as the start point and the end point. The sigmoidal decreasing function is used for the bare land, water body and residential classes, and sigmoidal increasing function is used for the rest of the classes (Figure.14). The averaged possibility value is then computed from the obtained fuzzy membership.

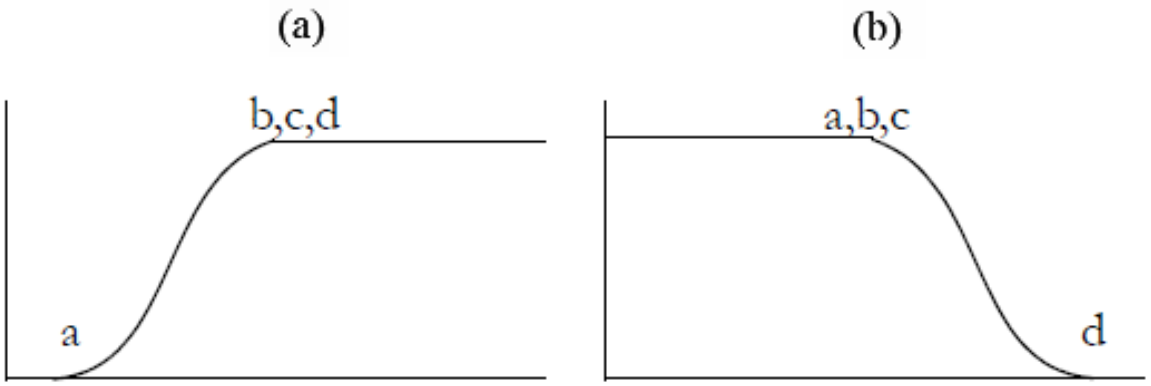

Figure 14. The sigmoidal membership function produced using a cosine function. The points a to d (along the x-axis) represents the inflection points governing the shape of the curve for (a) monotonically increasing shape and (b) monotonically decreasing shape.

The minimum VCI value and the maximum value used for each class as the inflection points, average degree of possibility for each land cover classes of the classified data and the reference data is listed in Table.7 and the average possibility values for each category were calculated by multiplying with the reference category and the classified category value to fit into the matrix (Table.8).

Table 7. List of the VCI value used in the fuzzy membership function, and the average fuzzy value computed for each of the classes of the classified map and the reference map.

	Classified VCI Min (a)	Classified VCI Max (b)	Reference VCI Min (a)	Reference VCI Max (b)	Average Fuzzy Value (Classified)		Average Fuzzy Value (Reference)	
					VCI_{mean}	$Fuzzy_{mean}$	VCI_{mean}	$Fuzzy_{mean}$
Coniferous	0.410134	0.96572	0.301876	0.977906	0.884192	0.948527	0.888412	0.94567
Silver Grass	0.560172	0.952448	0.265581	0.950968	0.829053	0.828093	0.852293	0.893879
Grasslands	0.390919	0.99717	0.295296	0.99717	0.76913	0.70294	0.779216	0.738551
Bare lands	0.0635	0.944625	0.111345	0.943727	0.655491	0.560937	0.469618	0.304187
Water bodies	0.048604	1	0.000002	0.940239	0.590886	0.533819	0.502571	0.333754
Crop lands	0.362285	0.944637	0.396596	0.952158	0.772072	0.619373	0.701587	0.722922
Paddy fields	0.000002	0.948069	0.244144	0.948178	0.673445	0.781971	0.663452	0.646427
Residential	0.222579	0.940738	0.153129	0.950462	0.618035	0.567961	0.548372	0.38621
Deciduous-Bl	0.707479	0.966771	0.353214	0.966771	0.901192	0.896936	0.916275	0.96095
Evergreen-Bl	0.446955	0.977906	0.308070	0.960948	0.892351	0.934219	0.89359	0.954593

Table 8. Each value represents the fuzzy value computed from the VCI for the accepted category given by: Average Fuzzy Value (Reference) × Average Fuzzy Value (Classified).

Classified \ Reference	Coniferous	Silver Grass	Grasslands	Bare lands	Water bodies	Crop lands	Paddy fields	Residential	Deciduous-Bl	Evergreen-Bl
Coniferous	-								0.9115	0.9055
Silver Grass		-	0.5821			0.5986				
Grasslands		0.6283	-			0.5082	0.4544			
Bare lands				-			0.3626	0.2166		
Water bodies					-		0.3451			
Crop lands		0.5536	0.4574			-	0.4004	0.2392		
Paddy fields		0.699	0.5775	0.2379	0.261	0.5653	-	0.302		
Residential				0.1728		0.4106	0.3671	-		
Deciduous-Bl	0.8482								-	0.8562
Evergreen-Bl	0.8835								0.8977	-

The value in the matrix is computed from calculating the mean fuzzy value of each category for the reference and the classified category and multiplying them together. This will be added with the score obtained from the questions generating a final score which will show the percentage of how many points should be considered as accepted, while the rest will be considered as poor (Table.9).

Table 9. The Probability of Chance Encounter (%) is computed to each of the categories which were accepted, by adding the scores from the questions and the value from the fuzzy set function. The percentages of the sample points in that category will be counted for the overall accuracy and for both producers and users accuracy.

Classified \ Reference	Coniferous	Silver Grass	Grasslands	Bare lands	Water bodies	Crop lands	Paddy fields	Residential	Deciduous-Bl	Evergreen-Bl
Coniferous	-								**59.115**	**59.055**
Silver Grass		-	**55.821**			**55.986**				
Grasslands		**56.283**	-			**55.082**	**54.544**			
Bare lands				-			**53.626**	**42.166**		
Water bodies					-		**43.451**			
Crop lands		**75.536**	**64.574**			-	**84.004**	**92.392**		
Paddy fields		**76.99**	**75.775**	**72.379**	**62.61**	**85.653**	-	**83.02**		
Residential				**41.728**		**64.106**	**63.671**	-		
Deciduous-Bl	**78.482**								-	**88.562**
Evergreen-Bl	**68.835**								**88.977**	-

The final output of the fuzzy error matrix is shown in Table.10 where the matrix is modified by separating the non-diagonal cells into accept and poor, and the points that belongs to “accept” are considered to be a “match” for estimating fuzzy accuracy. Fuzzy overall accuracy has resulted 79.3 % for the same land cover map which the accuracy was assessed in the conventional error matrix (55.5 %). This method is an alternative way of considering the accepted and poor, in the situation of if the accuracy assessment is based on a third party reference data and not by the primary ground data which has been collected at site. This method implies the consideration of the misclassification caused by the known physical explanation and the interpreter’s variability by weighting them. While it also considers the issue of the appropriateness of the sample unit, especially the problems stated when using the single pixel as the sample unit (Congalton and Green, 2009).

Table 10. Fuzzy Error Matrix following the same methodology as traditional error matrix with the following additions: Non-diagonal cells in the matrix contains accepted and poor. While the numbers in the accepted are considered a "match" for estimating fuzzy accuracy, the numbers in the poor was considered as an error. The fuzzy overall accuracy is estimated as the percentage of sites where the acceptable reference labels matched the classified label.

		Reference																				Users Accuracy	
		Coniferous		Silver Grass		Grasslands		Bare lands		Water bodies		Croplands		Paddy fields		Residential		DBL		EBL		Total Fuzzy	Percent Fuzzy
		Accept	Poor	Accept	Poor	Accept	Poor	Accept	Poor	Accept	Poor	Accept	Poor	Accept	Poor	Accept	Poor	Accept	Poor	Accept	Poor		
Classified	Coniferous	**9305**	0	0	100	0	52	0	16	0	61	0	125	0	158	0	39	**642**	444	**911**	632	10858/12485	86.97%
	Silver Grass	0	6	**365**	0	**27**	21	0	7	0	2	**4**	3	0	3	0	1	0	17	0	0	396/456	86.78%
	Grasslands	0	69	**108**	84	**211**	0	0	17	0	8	**47**	39	**39**	32	0	26	0	65	0	18	405/763	53.1%
	Bare lands	0	5	0	10	0	14	**41**	0	0	12	0	5	**4**	3	**25**	34	0	3	0	2	70/158	44.07%
	Water Bodies	0	5	0	9	0	2	0	12	**279**	0	0	0	**3**	5	0	6	0	1	0	14	282/336	84.07%
	Croplands	0	179	**22**	7	**43**	24	0	52	0	28	**235**	0	**199**	38	**182**	15	0	42	0	71	681/1137	59.92%
	Paddy fileds	0	309	**99**	29	**98**	31	**79**	30	**140**	83	**185**	31	**1339**	0	**290**	59	0	120	0	105	2229/3027	73.62%
	Residential	0	5	0	15	0	40	**23**	32	0	70	**22**	12	**66**	38	**651**	0	0	7	0	9	762/990	76.97%
	DBL	**934**	256	0	363	0	129	0	18	0	4	0	85	0	73	0	12	**1788**	0	**443**	57	3165/4162	76.04%
	EBL	**1194**	540	0	77	0	89	0	25	0	16	0	257	0	108	0	44	**999**	124	**1729**	0	3922/5202	75.39%
Producers		11433/12807		594/1288		379/781		143/352		419/703		493/1050		1650/2108		1148/1384		3429/4252		3083/3991		Fuzzy Overall Accuracy	
Accuracy		89.27%		46.12%		48.53%		40.63%		59.60%		46.95%		78.27%		82.95%		80.64%		77.25%		22771/28716=79.30%	

4.4. CO_2 Sequestration by Forests in Oita Prefecture

Referring to the observation by Tadaki & hachiya (1968), CO_2 sequestration by each forest types were calculated (Table.11). It has resulted total sequestration of coniferous forests at; 3.56 $MtCO_2$/yr, deciduous broad leaf forests; 0.77 $MtCO_2$/yr, and evergreen broad leaf forests; 2.25 $MtCO_2$/yr, totaling 6.59 $MtCO_2$/yr for all the forest cover together.

Table 11. CO_2 sequestration by each forest types of the study area.

Forest Type	**CO_2 Sequestration (tCO_2/ha/yr)** (Tadaki & Hachiya, 1968; Shida, 2007)	**Area (ha)**	**Total CO_2 Sequestration (tCO_2/yr)**
Coniferous	13.5 ±4.2	264,152	3,566,052
Deciduous-BL	8.7 ±3.0	89,208	776,109
Evergreen-BL	18.1 ±3.0	124,494	2,253,341
Total		477,854	6,595,502

4.5. CO_2 Sequestration by Forests in Oita Prefecture per Tree Age

4.5.1. Sequestration per Tree Age based on NDVI

For a deeper consideration of estimation of the coniferous forests, it was classified into per tree ages using the NDVI. On the left of Figure.15, shows the NDVI image for the study area. This is then reclassed into an image where each class representing ranges of the NDVI value (Figure.15 on the right). Each value range represents which age the coniferous tree would be according to Ishii (2007).

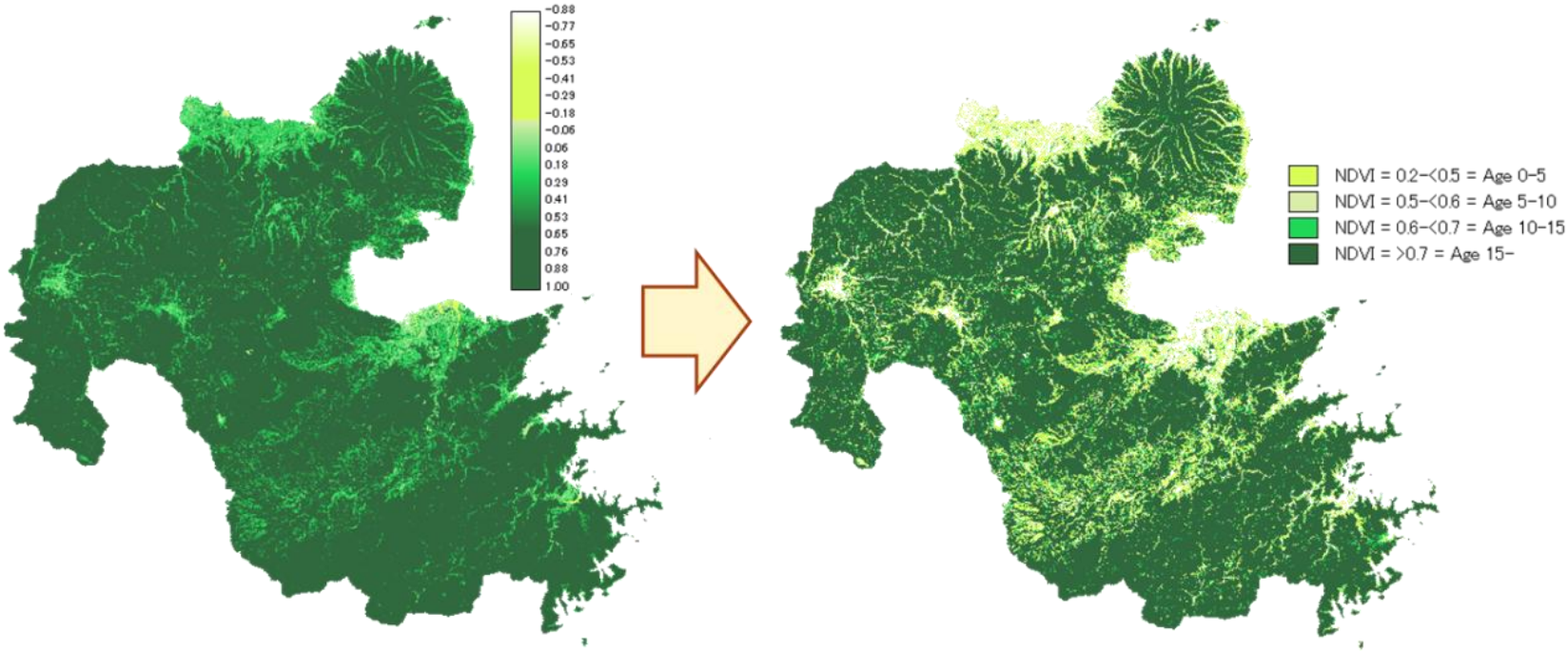

Figure 15. Original NDVI image of the study area on the left, and the reclassed NDVI image on the right. The range of NDVI is compatible with the Sugi tree ages.

This reclassed NDVI image is overlayed with the boolean image of a coniferous area so that the coniferous area for per tree ages can be extracted. As shown in Table.12, the tree age was classified into 4 ranges and the sequestrations per ages were calculated from the CO_2 sequestration table published by Tochigi Prefectural Government (2010). The total sequestration of the coniferous forests has resulted 2.35 $MtCO_2$/yr, comparing with when the averaged value was used for per forest type, the resulting value has decrease more than 34 %. However, when we see the sequestration value for per tree ages, the value shown in the 10-15 year coniferous trees are the ones that sequestrate CO_2 the most among other ages and contributing to the concept of carbon sink. It is also very similar to what was applied for the per forest type value, meaning that the averaged value used for per forest types can be a problem for overestimating the forests potential capacity and it is not good when we need a precise estimation for the carbon capacity.

Table 12. CO_2 sequestration of the *Sugi-Hinoki* forest area per tree ages.

Coniferous Age	CO_2 Equivalent (tCO_2/ha/yr) (Tochigi Prefecture, 2010)	Area (ha)	CO_2 Equivalent (tCO_2/yr)
0-5	0.6	15	9
5-10	4.8	1,316	6,317
10-15	13.5	11,772	158,922
15-50	8.7	251,048	2,184,118
Total		264,151	2,349,366

4.5.2. Sequestration per Tree Age based on Stem Volume

The stem volume map was produced using the backscattering intensity derived from the PALSAR data (Figure.16). Regarding to the stem volume table provided from the Oita Prefectural Government (modified and shown as a graph on Figure.17), the stem volume map was reclassed to the ranges of stem volume which will represent the range of ages. The range of the stem volume was reclassed considering the different growth rate among the regions of the study area. We found that in the Hita region, on the western region of Oita Prefecture, the coniferous forests in the age of 15-20 is more distributed among this area, while the age over 20 is distributed all along the Prefecture except for the Hita region. This could be understood by the features of Hita region, because they implement continuous afforestation activities and is very famous for forestry (wood products, etc.). However, in the other regions of Oita, the forests are left without any treatment so it shows older ages of the forests. For the deciduous forests, it is mostly a natural forest, so the distribution of the forests is mainly in the years over 30 (it is left naturally without human activity) and distributed all around Oita Prefecture.

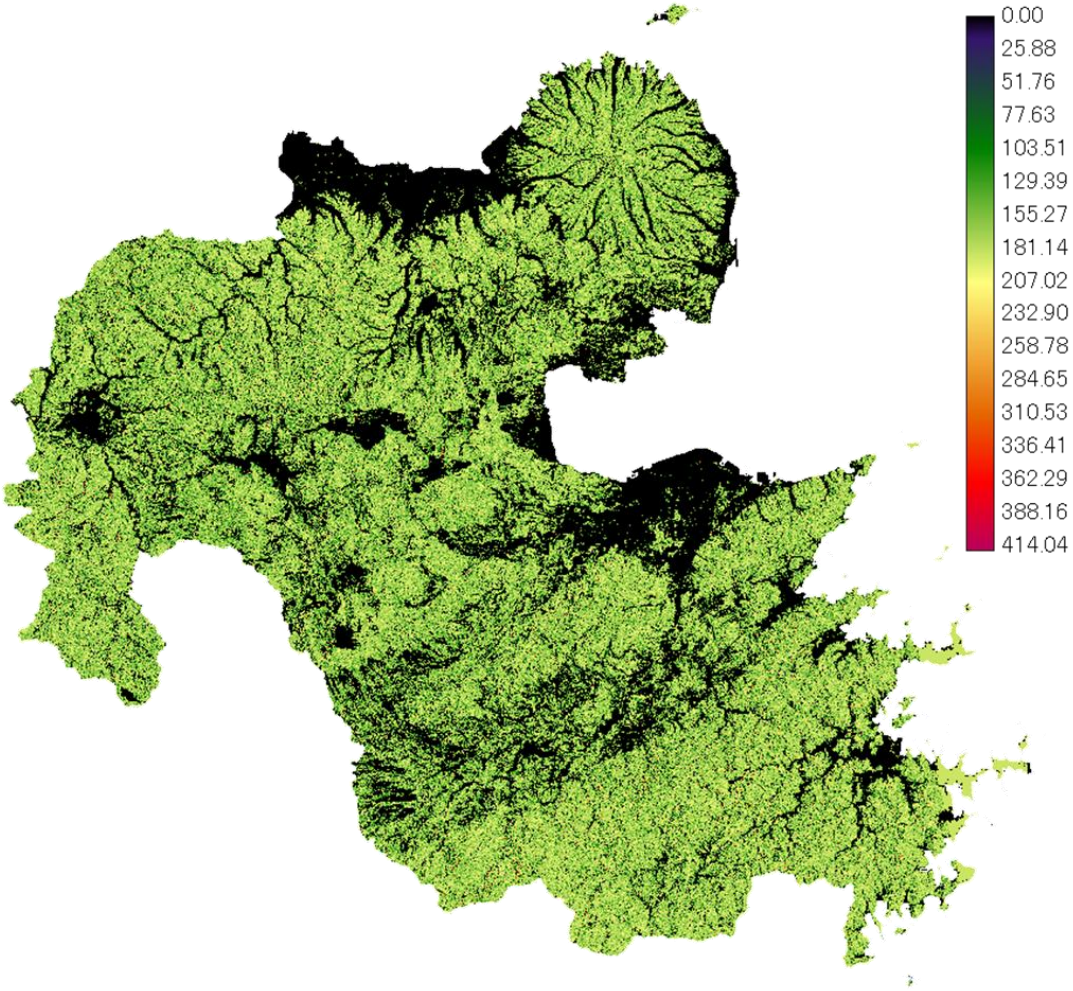

Figure 16. Stem Volume Map of the study area (m^3/ha).

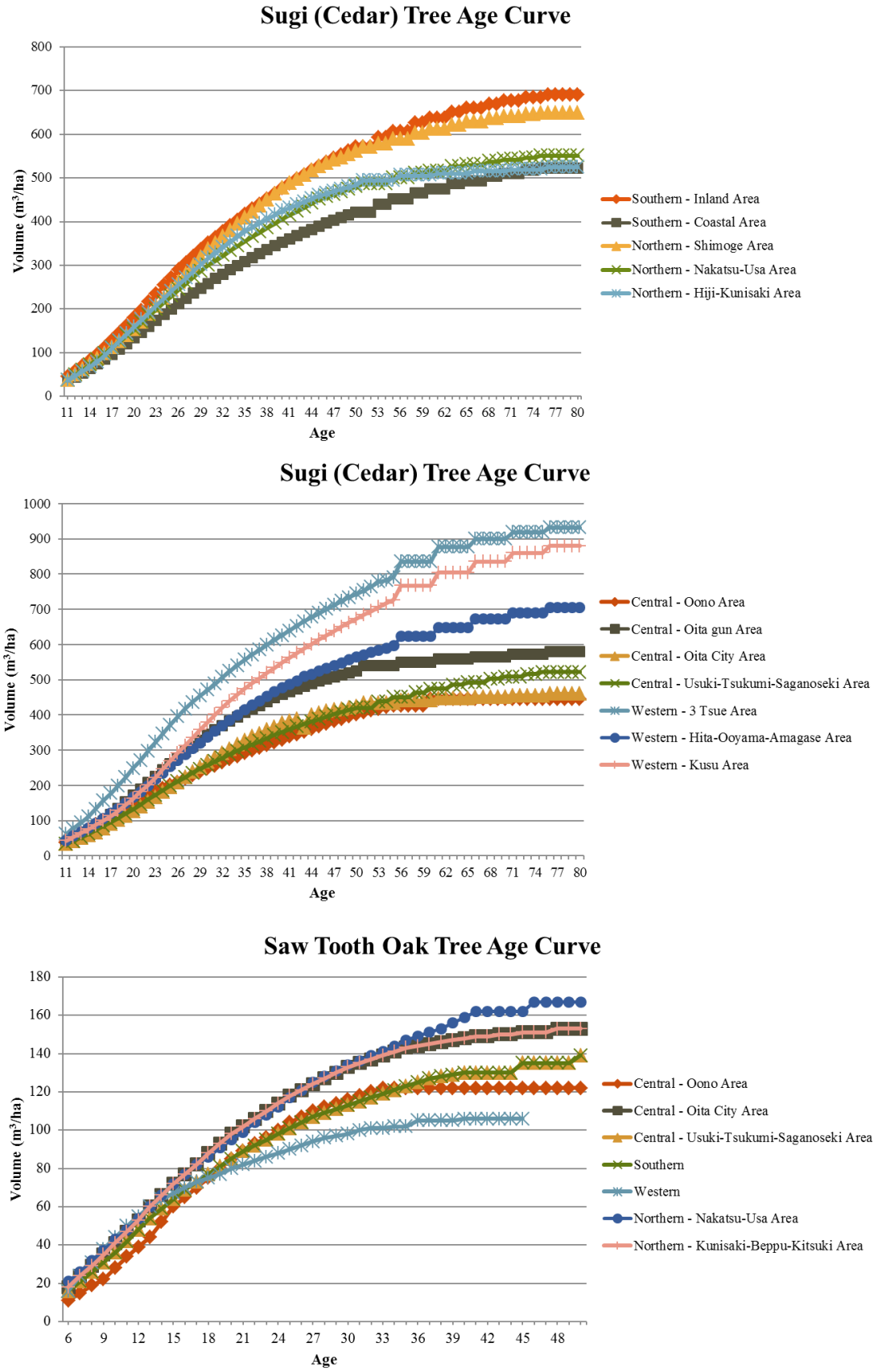

Figure 17. Stem volume as a function of tree age. The Sugi (Cedar) tree age curve on the top and Saw Tooth Oak on the bottom (Oita Prefecture). The growth of stem volume varies among different regions of the study area.

Again the coniferous forests was analyzed so that it can be compared with the results from the NDVI although, the ranges of the ages are more specific than the NDVI estimation. In addition, the deciduous broad leaf forests were analyzed also. The reason ages for the forests are more complex or more precise in other words, is because the saturation point for the NDVI and the stem volume map differs. The NDVI value after 0.7, the value saturates and shows the similar value for the ages above so there is a difficulty in classifying the tree age after 15 years. For the stem volume, it can be said the same only the saturation point is higher than the NDVI and it can sense the stem volume up to a certain point while after that, the value also saturates. The saturation point is mentioned by many researchers (Luckman et.al, 1998; Wijaya, 2009). The longer the wavelength, the more dense volumes can be observed, so if we need to observe more highly dense volumes we need a longer microwave such as the P-band SAR. Table.13 shows the results of the estimation. When we compare the estimation of the coniferous with the estimation made with the NDVI, the total sequestration has increased. This is because the sequestration value which was averaged after the age of 15 was considered up to year 50 which includes the values that sequester less. While the stem volume estimate can classify more precisely and the values are not averaged with the less sequester ages (like age 50), so it gives more amount from the earlier ages (15 to 20 and 20 to 25), resulting more sequestration compared with the NDVI estimation.

Table 13. CO_2 sequestration of coniferous and deciduous broad leaf forests per tree age.

Coniferous **Age**	**CO_2 Sequestration (tCO_2/ha/yr) (Tochigi Prefecture, 2010)**	**Area (ha)**	**Total CO_2 (tCO_2/yr)**
0-5	2.9	3,184	7,323
5-10			
10-15	13.5	8,941	112,657
15-20	14.8	90,441	1,293,306
20-25	11.3	147,084	1,500,257
25-30	10.2	5,358	46,615
30-50	6.4	662	3,972
Total		**255,640**	**2,964,130**
Deciduous-Bl **Age**			
0-5	5.5	310	1,705
5-10	9.4	614	5,772
10-15	8.2	1,205	9,881
15-20	8.2	1,557	12,767
20-25	5.9	2,168	12,791
25-30	5.8	2,709	15,712
30-50	3.2	78,044	249,741
Total		**86,607**	**308,369**

5. Discussions

5.1. Land cover Map

Producing a land cover map was made not only defining the areas as simple forests and non-forested area, but more in details (i.e. subclasses) such as for forests; coniferous, deciduous or even more classes, so that the information could be used and applied in various ways. Sanga-Ngoie (2003) has stressed on the need to produce a detailed digital land cover (or DVM) map, especially for the vegetation categories, in order to allow for more precise estimations of CO_2 sequestration values. We have examined various combinations and data to see which makes the best result for a high accurate land cover map. Single dataset for producing land cover map may be difficult especially when there are needs to clarify the vegetation's into details. If we look at the spectral signature (Figure.12), in the case of evergreen broadleaf forests and deciduous broadleaf forests for example, it is very hard to differentiate these two classes since they are similar in the May data. But, when it comes to the December data, the evergreen broadleaf (Live Oak) gives more radiance values than the deciduous forests, and this is caused by the seasonal change in the forests where the leafs gets fallen for the deciduous while the leafs remain on evergreen forests. These differences can distinguish the various classes where it makes hard to classify, and that is why we have used this method. Even from the numbers, we can see the improvements made from using temporal data, where for the single data and non-corrected image, it was resulted at 40 %, 14 % and 22 % accuracy for coniferous, deciduous and evergreen broad leaf forests respectively, and the use of temporal data and corrected image resulted at 73 %, 42 % and 44 % for coniferous, deciduous and evergreen broad leaf forests respectively. If the data sets are available, and the required needs are completed it is recommended to use temporal data for improving the land cover map.

5.2. Accuracy Assessment

Accuracy assessment in the remote sensing world has been common with the use of conventional error matrix for checking the reliability of the land cover map. Not many people take attention to the information from the error matrix but rather more on the overall accuracy. Congalton and Green (1993) recommend the error matrix as a jumping off point for identifying sources of confusion (i.e. differences between the map created from remotely sensed data and the reference data) and not simply the error. If we take an example from the error matrix computed on this study (Table.5), the reference class of "water bodies" gets confused with the "paddy fields". This is well understood, because depending on the season of the data, the paddy field might be filled with water which will give similar spectral signature to the water bodies and even by the human interpretation, especially when defining it by airborne photo, there might be confusions and that will lead to errors in the process of producing the reference map and which will again give errors to when using that reference map as a ground truth. Accuracy assessment can be a process to locate the error and to understand the problem of the misclassification for to prevent. It should be more taken attention than just only the overall accuracy.

However, in this study not only the conventional accuracy assessment but we have applied the fuzzy accuracy assessment also, to compare how different it will make when we fuzz the boundaries of the classes. The steps taken in this study was different from the method developed by Green and Congalton (2004). They have assigned each class to be evaluated as acceptable or poor based on fuzzy rules and we have set similar rules but only in the way of weighting the rules into series of questions and using the VCI method to compute degree of acceptance for each class. Conventional accuracy assessment is a common process for the remote sensing society, but to consider more of the reality or the complexity of the environment, we suggest that fuzzy accuracy assessment should be implemented as if the conventional accuracy assessment is done for any classification scheme. The method developed here should simplify the process for applying fuzzy accuracy assessment to compute the fuzzy overall accuracy, although even it is trying to remove the human interpretation and misclassification errors, the questions for the weights to choose is already depending on the users interpretations. There needs to be improvements made in this process by asking the experts for the criterions or develop a method to evaluate the degree of acceptance in a full quantitative way.

5.3. Result of the Sequestration

Recently, the Oita Prefectural Government has estimated the sequestration by the forests of Oita (Oita Prefecture Global Warming Measure, 2010). They have differentiated the forests into natural and planted forests and calculated the sequestration value as same as how it is calculated in the IPCC guideline (IPCC, 1996). The equation is used below:

$$\text{Annual Carbon Sequestration} = \text{Annual Growth } (m^3/ha) \times \text{Magnification Factor} \times \text{Bulk Density} \times \text{Carbon Content} \quad (17)$$

Magnification Factor is a factor for expanding the stem volume to estimate the whole volume of the tree which includes the volume of all leafs, branches and roots together. The magnification factor gives a value of 1.7 and 1.8 for coniferous trees and broadleaf trees, respectively. However, the value varies among trees due to tree age and so forth, although it is a common value used and implemented anywhere in Japan. Bulk density is representing how much weight a tree with a size of 1 m^3 has and it will depend on the tree types. Roughly, carbon content is said to be 0.5, which means the composition of wood contains 50 % of carbon and it is a common value used even by the IPCC (1996). To obtain the total sequestration by the forests, the total area will be multiplied with equation (17). To convert carbon sequestration to CO_2 sequestration, simply multiply 44 divided by 12, which is the molecular mass of the carbon (12) and CO_2 (44 (Oxygen = 16)).

The result was that they are likely to sequester 2.07 $MtCO_2/yr$. However in our result it has been estimated at 5.52 $MtCO_2/yr$ considering the forests type and tree ages, which is the potential value for all the forests of Oita Prefecture and when considering the eligible amount of sequestration it is estimated at 3.87 $MtCO_2/yr$ (multiplied the forest management rate = 0.7). Of course when estimating the eligible amount, it would be lesser than the potential value,

although, it is more than what has been estimated by the prefectural government. It has shown that there are uncertainties in the method taken by the Prefectural Government. The method they use gives sequestration value from 3.32 tCO_2/ha/yr to 6.72 tCO_2/ha/yr range (tree type considered as planted or natural forests) which is very low from what has been observed by researchers (among various tree types), and even in this study we have shown the diversity in the ranges of sequestration among tree ages which we believe it is more likely close to the real CO_2 sequestration value.

When looking through the sequestration value for tree ages, the 10-15 year of the coniferous forests matches with the averaged coniferous value for the forests types, similar with the deciduous broad leaf forests. It means that if the estimation is made based on the averaged value, it will neglect the other trees in a different growth rate, and there might be a possibility of overestimating the carbon sink capacity. Conventional method of estimating sequestration is done by multiplying the averaged sequestration value per unit area by the total forests area which was also implemented in this study. Although as mentioned, sequestration differs among ages also, and it needs to be considered because otherwise it will not give us the true value of the forests capacity. Two methods were used to analyze the tree ages. One is using NDVI, and the other is estimating from the stem volume. Stem volume showed the most precise estimation because it has covered the ages from 0 to 30 years in 5 year interval and over 30 year range. Both methods have showed a decrease of sequestration from when applying the averaged value. It's a matter of fact, the sequestration amount will change its result from what range of age is distributed the most and that result can be analyzed more precise by using the backscattering intensity information derived from the PALSAR data. The methodology developed here by using the land cover map to locate the resource and utilize the PALSAR data to derive the information of the stem volume has performed a well process for quantifying the forests carbon capacity for the interest of global warming and forests resource management. The use of remote sensing has a strong advantage of understanding where and what type of resource there is and the status of those. The status of the resources, in this case the tree ages or the stem volume information, not only it could lead to more precise estimation but it is important information when it comes with timber products, because the percent of acceptance to grade requirements increases with tree age (Bibilis et.al, 1993).

So, as a result, we recommend the method developed in this study for more precise and detailed information of the environment and estimating CO_2 sequestration. For the sequestration, Oita Prefectural Government is underestimating the forests capacity, and if they are taking to consider the concept of carbon sink as for their countermeasure plan, it has to be known that their estimation is wrong. Wrong results could lead to wrong decision makings and that needs to be strongly avoided.

5.4. Stem Volume Estimation and PALSAR Correction

The estimation of the stem volume was computed using the backscattering intensity derived from the PALSAR data and applying the model which was developed by Wijaya (2009) using the data from Indonesia. The issue is that, we know the backscattering signature gets affected

by the moisture of the soil, or the topography, and so on. It is here a question marked how good this model applies to the study area, because the climate conditions and the vegetation's are different. This could be answered in the future works, while many researchers analyze the correlation between the backscatter and the stem volume or biomass with different polarizations with the same forested area but they do not look through the backscattering signature among different vegetation's for different polarizations. This needs to be examined so that we could see if there are any differences, and if there are it means we need to develop a model that coincide with the Japanese forests.

The issue of correcting the positioning of the PALSAR image is another issue especially when it needs to be fused with the optical images, this problem can lead to errors such as when constructing the training sites. Because of the positioning problem, the training sites do not match the coordinates between the optical and the SAR data and that makes an error to the information of spectral signatures for each land classes. The only little significance of the land cover map when fusing the PALSAR data in the classification process could be resulted from this issue. Ortho-rectification is the method for to overcome with this although it was not implemented in this research. The correction of the PALSAR image using the methods of Castel et.al (2001) has an issue that does not take in account, which is some basic problem of the SAR data; the layover and shadowing effects. Especially in Japan, because there are many mountains and slopes, without treatment of these effects, it is difficult to even make comparison of backscatter from various sites and/or multiple satellites, etc. Small (2011) has developed an new method that improves the normalization of the SAR image which considers the effects of the layover and shadowing and it could be one method for overcoming with the issue and improving the results of what has been done here. This method could give us more options to the data to be acquired, such as even if the image was obtained in an ascending mode or descending mode or in any other modes. Correction of the images are an critical issue for obtaining the true value of the area, and without that, any results that is obtained may turn out to be wrong.

5.5. Decision Making

According to what we have found through this research, we think that Oita Prefecture can devise better scenarios for mitigating the global warming issue. The location of the resources could be known using the satellite remote sensing data, while the status of the resources could be analyzed using the SAR data. The sequestration per ages is known, and it is shown that around 10 to 25 years gives the highest sequestration rate. Even using the information that was hidden at the Prefectural Government, the growth rate of the trees among different regions is observed. So, as a result, we can imply for the afforestation plans by considering the areas of forests that could be replaced with new trees in a region where it could grows the fastest. Of course the issue of the timber products needs to be checked if it could be used as a product for the 20 to 25 year trees, but these information's which was outputted could be an strong information for the Prefectural Government for them to make decisions and for to take actions.

6. Conclusions

This research has employed LANDSAT ETM+ and ALOS PALSAR data from a series of dates and field data collected at Oita Prefecture, Japan, to estimate the CO_2 sequestration potential of the forests in Oita. Fusion of the optical and the microwave data has resulted with comparable results to other estimation methods and the estimation made by the prefectural government. Total CO_2 estimation resulted at 5.52 $MtCO_2$/yr when the forest types and tree ages were considered (coniferous; 2.96 $MtCO_2$/yr, deciduous broad leaf; 0.31 $MtCO_2$/yr, evergreen broad leaf; 2.25 $MtCO_2$/yr). Final product of the land cover map has resulted at 55.5 % and 79.3 % for overall accuracy and fuzzy overall accuracy respectively. It was shown that the accuracy has improved by correcting the satellite imagery and by using temporal data of the study area and little significant has been seen fusing the PALSAR data depending on the combination of the images. Although, the overall accuracy should be little more improved so that the reliability of the output results could be more confident. The sequestration value is a problem since that averaged value will give big differences among less sequester regions or larger regions, even in this case, the value for Oita Prefecture should be used however, lack of scientific data is also generating the problem for the estimation. Climatic or geographical conditions differ among regions, and it will make differences to the sequestration so each Prefectural Government should observe the sequestration for their own region and output the data. By combining the optical and SAR remote sensing data, it is possible to estimate precise carbon capacity, or the realistic amount sequestered by the forests. The location of the resources and the detail information of the status of the forests can provide information's for the decision makers to implement more effective policies and for to take actions.

For the future works, the method will be applied to all the regions of Japan to estimate the actual sequestration the forests are taking as whole of Japan. The investigation of this would give strong information to the Japanese Government for implementing various measures related to the global warming issue and forests resource managements.

Acknowledgments

We are very grateful to the members and the faculty of the laboratory of Environmental Geoscience, Graduate School of Asia Pacific Studies, Ritsumeikan Asia Pacific University and the members of the ENVOL for the informative remarks and suggestions during the elaboration of this work. We kindly appreciate the professors who have given us informative comments and advise to brush up the content of this work. We also thank Oita Prefectural Government, Forest Management Division Department of Agriculture Affairs for providing the stem volume data.

References and Notes

1. Armston J, Carreiras J, Lucas R and Shimada M (2010) ALOS PALSAR backscatter mosaics for Queensland, Australia. Proceedings of the 15th Australasian Remote Sensing & Photogrammetry Conference. September 2010, Australia
2. Bibilis E.J., Brinker R., Carino H.F. and Mckee C.W. (1993) Effect of stand age on flexural properties and grade compliance of lumber from loblolly pine plantation timber. *Forest Products Journal, Vol.43*, pp. 23-28
3. Bird M. (2010) Monitoring the carbon cycle in Tropical forests. *Environmental Opinion Leaders for the Asia Pacific 2010 International Symposium Official Report*, Ritsumeikan Asia Pacific University, Japan, pp. 39-54
4. Brown de Colstoun Eric C, Story Michael H, Thompson C, Commisso K, Smith Timothy G and Irons James R (2003) National Park vegetation mapping using multitemporal Landsat 7 data and a decision tree classifier. *Remote Sensing of Environment, Vol.85*, pp. 316-327
5. Champion I, Dubois-Fernandez P, Guyon D, Cottrel M. (2008) Radar image texture as a function of forest stand age, *International Journal of Remote Sensing, Vol.29, No.6*
6. Chen E., Li Z., Ling F., Lu Y., He Q. and Fan F. (2009) Forest Volume Density Estimation Capability of ALOS PALSAR Data over Hilly Region. *Proc. of 4th International Workshop on Science and Applications of SAR Polarimetry and Polarimetric Interferometry – PolInSAR 2009*, January 2009, Italy
7. Chiras D.D. (2006) Environmental Science Seventh Edition, Jones and Bartlett, United Kingdom, p.458
8. Congalton R.G. & Green K. (1993) A practical look at the sources of confusion in error matrix generation. *Photogrammetric Engineering and Remote Sensing. Vol.59, No.5*, pp.641-644.
9. Congalton R.G. & Green K. (2009) *Assessing the accuracy of remotely sensed data; principles and practices*, second edition.; CRC/Taylor & Francis: New York; pp. 70-74
10. Eastman J. Ronald (2006) *IDRISI Andes Guide to GIS and Image Processing*, Clark Labs, Clark University, p.176
11. Gopal S. and C. Woodcock (1994) Theory and methods for accuracy assessment of thematic maps using fuzz sets. *Photogrammetric Engineering and Remote Sensing, Vol.60, No.2*, pp. 181-188
12. Green K. and R. Congalton (2004) An error matrix approach to fuzzy accuracy assessment: the NIMA Geocover project. A peer-reviewed chapter in Lunetta, R.S. and J.G. Lyon (Eds.), *Remote Sensing and GIS Accuracy Assessment*, CRC Press, Boca Raton, FL.
13. Hewitt C.N. and Jackson A. (2003) Handbook of Atmospheric Science: Principles and Applications, Blackwell, United Kingdom, pp. 368-370
14. Hiroshima & Nakajima (2006) Estimation of sequestered carbon in article-3.4 private planted forests in the first commitment period in Japan. *Journal of forest research, Vol.11, No.6*, pp.427-437

15. J. R. Holton (1992) An Introduction to Dynamic Meteorology Third Edition, Academic Press, California
16. IPCC (1996) Revised 1996 IPCC Guidelines for National Greenhouse Gas Inventories. J.T. Houghton, L.G. Meira Filho, B. Lim, K. Treanton, I. Mamaty, Y. Bonduki, D.J. Griggs, and B.A. Callander (eds.). Intergovernmental Panel on Climate Change, Meteorological Office, Bracknell, United Kingdom.
17. Ishii T. (2007) Estimation of forest leaf area index using remote sensing data and its applications to predicting forest carbon sequestration and water budget (Japanese)
18. Janssens Ivan A, Freibauer A, Ciais P, Smith P, Nabuurs G-J, Folberth G, Schlamadinger B, Hutjes Ronald W. A, Ceulemans R, Schulze E-D, Valentini R and Dolman A. J (2003) Europe's Terrestrial Biosphere Absorbs 7 to 12% of European Anthropogenic CO_2 Emissions. *Science. Vol.300, No.5625* pp. 1538-1542
19. Karjalainen M, Pyysalo U, Karila K and Hyyppa J (2008) Forest Biomass Estimation using ALOS PALSAR Images in Challenging Natural Forest Area in Finland. *Proc. of the ALOS PI 2008 Symposium*, November 2008, Greece
20. Kato M. (2004) Forestry Remote Sensing - Basics to Application. Japan Forestry Investigation Committee, Toyko (in Japanese)
21. Kobayashi S. & Sanga-Ngoie K. (2008) The integrated radiometric correction of optical remote sensing imageries, *International Journal of Remote Sensing Vol.29, No.20*
22. Kogan F.N. (1998) A typical pattern of vegetation conditions in southern Africa during El-Niño years detected from AVHRR data using three-channel numerical index. *International Journal of Remote Sensing, Vol.19, No.18,* pp.3689-3695.
23. Kuplich T.M, Salvatori V, Curran P.J. (2000) JERS-1/SAR backscatter and its relationship with biomass of regenerating forests, *International Journal of Remote Sensing Vol.21, No.12*
24. Lo, C. P. and Choi, J. (2004) A hybrid approach to urban land use/cover mapping using Landsat 7 enhanced thematic mapper plus (ETM+) images. *International Journal of Remote Sensing, Vol.25*, pp. 2687-2700
25. Luckman A, Baker J, Honzak M and Lucas R (1998) Tropical Forest Biomass Density Estimation Using JERS-1 SAR: Seasonal Variation, Confidence Limits, and Application to Image Mosaics. *Remote Sensing of Environment, Vol.63*, pp. 126-139
26. MAFF (Ministry of Agriculture, Forestry and Fisheries) (2010) Function of the sequestration of forests/trees, *Available online at: http://www.rinya.maff.go.jp/kinki/hyogo/mori-grow/mori-co2.html (2011/4/10 accessed)* (Japanese)
27. Matsumoto M. (2001) Carbon Stock and Carbon Sequestration by the Forests of Japan, *Shinrin Kagaku, 33* (Japanese)
28. METI (Ministry of Economy, Trade and Industry) (2005) Kyoto Protocol Target Achievement Plan, *Available online at: http://www.meti.go.jp/policy/energy_environment/global_warming/study_policy.html* (2011/7/12 accessed) (Japanese)

29. OECD (Organization for Economic Co-operation and Development) (2004) Environmental Data Compendium, Forest. *Available online at: http://www.oecd.org/document/40/0,3746,en_2649_34283_39011377_1_1_1_1,00.html (2011/4/10 accessed)*
30. Oita Prefecture Forestry Figures (2003) *Available online at: http://www.pref.oita.jp/site/toukei/h1506.html (2011/4/10 accessed)* (Japanese)
31. Oita Prefecture Global Warming Measures (2006) *Available online at: http://www.pref.oita.jp/uploaded/life/111018_123085_misc.pdf (2011/06/28 accessed)* (Japanese)
32. Oita Prefecture Global Warming Measures (2010) *Available online at: http://www.pref.oita.jp/soshiki/13020/ondan-keikaku.html (2011/06/28 accessed)* (Japanese)
33. Richards J.A & Jia X. (1999) *Remote Sensing Digital Image Analysis: An Introduction. Third, Revised and Enlarged Edition.*; Springer; New York
34. G.H. Rosenfield and K. Fitzpatrick-lins (1986) Remote Sensing and image interpretation. John Wiley & Sons, New York
35. Sanga-Ngoie K. (2003) Quantitative estimation of CO_2 sequestration by forest systems in Mie using GIS and Remote Sensing, *2003 Annual Conference for The Mie University GIS Society: GIS and Remote Sensing -Powerful tools for eco-climatic analysis- Vol.3,* pp.75-78
36. Sanga-Ngoie K. and Kobayashi S. (2003) A perspective on the integration of the land-use/land-cover classification results using GIS and LANDSAT data. 2*003 Annual Conference for The Mie University GIS Society: GIS and Remote Sensing -Powerful tools for eco-climatic analysis- Vol.3,* pp.69-74 (Japanese)
37. Santoro M, Fransson J.E.S, Eriksson L.E.B, Magnusson M, Ulander L.M.H and Olsson H (2009) Signatures of ALOS PALSAR L-Band Backscatter in Swedish Forest. *IEEE Transactions on Geoscience and Remote Sensing, Vol.47, No.12*
38. Santoro M, Beer C, Cartus O, Schmullius C, Shvidenko A, McCallum I, Wegmuller U and Wiesmann A. (2011) Retrieval of growing stock volume in boreal forest using hyper-temporal series of Envisat ASAR ScanSAR backscatter measurements. *Remote Sensing of Environment Vol.115,* pp.490-507
39. Sasaki N and Kim S (2009) Biomass carbon sinks in Japanese forests: 1966-2012. *Forestry, Vol.82, No.1*
40. Small D. (2011) Flattening Gamma: Radiometric Terrain Correction for SAR Imagery. *IEEE Transactions on Geoscience and Remote Sensing. Vol.49, No.8,* pp.3081-3093.
41. Tadaki Y. and Hachiya K. (1968) Forest ecosystems and their productivity, *Ringyo Kagakugijutsu Shinkosho, p.64* (Japanese)
42. Tucker, C.J. (1979) Red and photographic infrared linear combinations for monitoring vegetation. *Remote Sensing of Environment, vol.8*, pp.127-150
43. Turner D P, Guzy M, Lefsky M A, Ritts W D, Tuyl S V and Law B E (2004) Monitoring Forest Carbon Sequestration with Remote Sensing and Carbon Cycle Modeling. *Environmental management, Vol.33, No.4*, pp. 457-466

44. The National Survey on the Natural Environment (6^{th} (1999-2004), 7^{th} (2005-)) *Available online at: http://www.vegetation.jp/ (2011/4/10 accessed)*
45. Ulander L.M.H (1996) Radiometric Slope Correction of Synthetic-Aperture Radar Images. *IEEE Transactions on Geoscience and Remote Sensing, Vol.24, No.5*
46. UNFCCC (1998) Kyoto Protocol to the United Nations Framework Convention on Climate Change, *Available online at: http://unfccc.int/resource/docs/convkp/kpeng.pdf (2011/06/28 accessed)*
47. USGS (United States Geological Survey) (2004) SLC-off Gap-Filled Products Gap-Fill Algorithm Methodology. *Available online at: http://landsat.usgs.gov/documents/L7SLCGapFilledMethod.pdf (2011/12/26 accessed)*
48. USGS (United States Geological Survey) (2010) SLC-off Products: Background. *Available online at: http://landsat.usgs.gov/products_slcoffbackground.php (2011/4/10 accessed)*
49. USGS (United States Geological Survey), Earth Explorer: Satellite Images, Aerial Photographs and Maps. *Available online at: http://edcsns17.cr.usgs.gov/NewEarthExplorer/ (2011/4/10 accessed)*
50. Wijiya A. (2009) Evaluation of ALOS-PALSAR Mosaic data for estimating stem volume and biomass: A case study from tropical rainforest of central Indonesia. *Jurnal Geografi, Vol.2, No.1*
51. Xiuwan, C. (2002) Using remote sensing and GIS to analyse land cover change and its impacts on regional sustainable development. *International Journal of Remote Sensing, vol.23*, pp. 107-124